The Somatic Golgi nucleates microtubules that are directed by Kinesin-2 to maintain microtubule polarity within neurons

Amrita Mukherjee[1], Paul Brooks[1], Fred Bernard[2], Antoine Guichet[2] and Paul T. Conduit[1,3]

[1]Department of Zoology, University of Cambridge, Downing Street, Cambridge, CB2 3EJ

[2]Université de Paris, CNRS, Institut Jacques Monod, - Bâtiment Buffon, 15 rue Hélène Brion, 75205 Paris CEDEX 13 - France

[3]Corresponding author

Paul Conduit

44-1223-334471

ptc29@cam.ac.uk

Abstract

Microtubules form polarised arrays throughout axons and dendrites necessary for neuronal growth and maintenance. γ-tubulin-ring-complexes (γ-TuRCs) nucleate microtubules at microtubule organising centres (MTOCs), but how microtubules are generated and organised within neurons remains unclear. We show that γ-TuRCs are predominantly recruited to the somatic Golgi, rather than to dendritic Golgi outposts, within *Drosophila* neurons. Microtubules nucleated from the somatic Golgi grow preferentially towards and into the axon, while growing microtubules that approach dendrites are excluded. Both directed growth and dendritic exclusion depend upon Kinesin-2, which associates with plus ends and directs their growth towards the plus ends of adjacent microtubules. We propose that plus-end-associated Kinesin-2 guides growing microtubules nucleated from the somatic Golgi towards the axon and prevents plus end entry into dendrites when engaging with oppositely polarised microtubules. In summary, microtubules are nucleated from the somatic Golgi within neurons and their guidance is necessary to maintain neuronal microtubule polarity.

Introduction

Microtubules are polarised polymers of tubulin essential for cell viability that provide pushing and pulling forces, structural support or tracks for the transport of intracellular cargo[1]. They are made from α/β-tubulin dimers that join end-to-end to form protofilaments, which associate laterally to form the hollow microtubule. α-tubulin is located at the so-called minus end and β-tubulin is exposed at the so-called plus end, which is typically more dynamic. This inherent polarity of microtubules is important for cell polarity, as different motor proteins (Kinesins and Dynein) move cargo along microtubules in a specific direction – Dynein towards the minus end and most kinesins towards the plus end. This is particularly relevant in neurons where nearly all of the plus ends in axons point away from the soma, known as plus-end-out or anterograde microtubules, while the microtubules in dendrites are of mixed polarity with a significant fraction of minus-end-out (retrograde) microtubules[2–4]. This difference in microtubule polarity is important for the correct distribution of cargo throughout the neuron[3–5].

Within cells *de novo* assembly of new microtubules i.e. microtubule nucleation is kinetically unfavourable and is catalysed by multi-protein γ-tubulin ring complexes (γ-TuRCs)[6]. These complexes provide a γ-tubulin-based template that promotes the lateral association of protofilaments during the initial stages of microtubule growth[7–9]. The single-turn helical pattern of 13 exposed γ-tubulin molecules is also thought to restrict the microtubule protofilament number to 13[7]. This avoids supercoiling of protofilaments that may otherwise prohibit long-range motor-driven transport along the microtubule, which is of clear importance in neurons. Knockdown of γ-TuRCs within model systems affects dynamic microtubules in all neuronal compartments[10–14] and mutations in γ-TuRC genes have been linked to human neurodevelopmental disorders[15–17].

γ-TuRCs assemble in the cytosol but they are typically inactive until recruited to specific sites, such as microtubule organising centres (MTOCs), the cytosol around mitotic chromatin or the sides of pre-existing microtubules via Augmin/HAUS[18–22]. A range of MTOCs exist, including centrosomes, the Golgi apparatus and the nuclear

envelope, and different cells use different MTOCs to help generate and organise their specific microtubule arrays[18]. γ-TuRC recruitment occurs via γ-TuRC "tethering proteins" that simultaneously bind to the MTOC and γ-TuRC, possibly also helping to activate the γ-TuRC. An example is *Drosophila* Centrosomin (Cnn) and its mammalian homologue CDK5RAP2, which recruit γ-TuRCs to centrosomes during mitosis[23–26] and whose binding can activate γ-TuRCs[27–29]. γ-TuRCs can be recruited to different MTOCs by different tethering proteins, and it was also recently shown that different isoforms of Cnn can mediate recruitment to different MTOCs[29]. Thus, there is potentially a wide-range of γ-TuRC recruitment mechanisms available and understanding which mechanisms are used in different cells, including neurons, remains poorly understood.

Although it is known that γ-tubulin is important[10–14], it remains unclear how microtubule nucleation is regulated within neurons. During early development of mammalian neurons, the centrosome within the soma nucleates microtubules[30] that are severed and transported into neurites via motor-based microtubule sliding[31]. Microtubules sliding is also important for axon outgrowth in *Drosophila* cultured neurons[32,33], and for establishing microtubule polarity[34–38]. Centrosomes are inactivated, however, at later developmental stages[30] and are dispensable for neuronal development in both mammalian and fly neurons[30,39]. No other active MTOCs within the neuronal soma have been described. Nevertheless, microtubules continue to grow within the soma[11,39], and in mammalian neurons this depends in part on HAUS[11], which is also important for microtubule growth within axons and dendrites[11,40]. Some MTOCs have been identified within dendrites in different neurons. For example, the basal body, or its surrounding region, within *C. elegans* ciliated neurons acts as an MTOC at the distal end of the dendrite[5]; this is also true of the URX non-ciliated neuron, but the identity of the MTOC is unclear[5]. Within the dendrites of *Drosophila* dendritic arborisation (da) neurons, fragments of Golgi called Golgi outposts have been proposed to recruit γ-TuRCs and act as MTOCs[12,41,42].

Drosophila da neurons are a particularly good model to study microtubule generation and organisation within neurons *in vivo*. Their cell bodies and dendritic arbors lie just

below the epidermis, making them ideal for imaging through the translucent body wall. They are specified during embryogenesis and are categorised into four classes based on their dendritic morphology, with class I neurons having the simplest branching pattern and class IV neurons the most elaborate[43]. Class I neurons are proprioceptive, detecting the peristaltic movements of the larvae, and thus have parallel dendrites that run in a specific anterior-posterior orientation forming a "comb-like" arbor. In contrast, class IV neurons are nociceptive, detecting external stimuli such as touch or heat, and they tile the surface of the larvae with each neuron displaying a dense branching pattern. In both neuronal classes, microtubules in axons are predominantly plus-end-out throughout development, but microtubule polarity in dendrites progressively becomes more minus-end-out as the neurons develop, such that by late larval stages the majority of dynamic microtubules are minus-end-out[44,49]. Microtubule polarity within da neurons can be disrupted under various mutant or RNAi knockdown conditions[10,12,41,42,45–48], but we still don't have a full understanding of how microtubule polarity is normally established and maintained.

Golgi outposts, which in both mammalian and *Drosophila* dendrites are involved in localised protein trafficking and membrane supply[50–55], appear to also regulate microtubule nucleation in *Drosophila* da neurons[12,41,42]. Golgi outposts are enriched at dendritic branch points[54,55] and studies in *Drosophila* suggest that microtubules nucleated from Golgi outposts help regulate dendritic branching and contribute to maintaining microtubule polarity[12,41,42]. Unlike the somatic Golgi, which in both mammalian cells and *Drosophila* comprises cis, medial and trans compartments organised into stacks and ribbons[56,58], Golgi outposts can be either single- or multi-compartment units with multi-compartment units having a higher propensity to initiate microtubule growth[42]. Within class I da neurons, Golgi outpost-mediated nucleation is thought to be dependent on the γ-TuRC-tethering protein Cnn and is thought to help restrict dendritic branching[41], while within class IV neurons Golgi outpost-mediated nucleation is thought to be dependent on Pericentrin-like protein (Plp) and is thought to help promote dendritic branching[12]. There remains some uncertainty, however, about the role of Golgi outposts in microtubule nucleation, as a separate study that examined the localisation of ectopically expressed γ-tubulin-GFP concluded that γ-

tubulin localises predominantly to dendritic branch points in a Golgi outpost-independent manner[10].

In this study, we aimed to identify sites of microtubule nucleation within *Drosophila* da neurons. We used endogenously tagged γ-tubulin-GFP as a proxy for γ-TuRCs and made a detailed analysis of γ-TuRC localisation within both class I and class IV da neurons. We find variation between neuronal classes in how γ-TuRCs localise within dendrites, but find that the most prominent localisation of γ-TuRCs is at the somatic Golgi within all sensory neurons of the dorsal cluster. This association of γ-TuRCs with the somatic Golgi is not dependent on either Cnn or Plp. Using an *in vivo* microtubule nucleation assay, we show that the somatic Golgi is a genuine site of microtubule nucleation. Moreover, we also found that microtubules initially grow preferentially towards the axon, suggesting that microtubule nucleation events at the somatic Golgi are asymmetric, and that growing microtubules turn towards the axon in a Kinesin-2 dependent manner. Growing microtubules readily enter axons contributing to plus-end-out microtubule polarity, but are excluded from entering dendrites to help maintain minus-end-out polarity within proximal regions of the primary dendrites. This dendritic exclusion is also dependent on Kinesin-2. We therefore propose a model to explain microtubule guidance towards axons, and dendritic exclusion, based on Kinesin-2's ability to associate with growing microtubule plus ends while simultaneously engaging with adjacent microtubules.

Results

A detailed analysis of endogenous γ-tubulin localisation within class I and class IV da neurons

We began by examining the localisation of γ-tubulin (as a proxy for γ-TuRCs) within class I and class IV da neurons. To avoid any potential artefacts induced by ectopic overexpression, we used alleles where γ-tubulin23C (the zygotic form of γ-tubulin) was tagged at its endogenous locus with GFP ([57] and this study). We generated fly stocks expressing two genetic copies of endogenously-tagged γ-tubulin23C-GFP (hereafter γ-tubulin-GFP) and the membrane marker mCD8-RFP, expressed either in class I or class IV da neurons, and imaged living animals. We found that γ-tubulin-GFP was not strongly enriched throughout the dendrites of either neuron (Fig. 1A; Fig. 2A), but that we could detect discrete accumulations of γ-tubulin-GFP at specific dendritic sites. This varied between class I and class IV neurons, so we describe each neuron in turn below.

For class I da neurons we focussed on the ddaE neuron (hereafter class I neurons), as these have been the most widely characterised. From 13 class I neurons analysed, we detected an average of 1.1 discrete γ-tubulin-GFP puncta per 100μm of dendrite (Fig. 1A). Most puncta were just above background intensity levels, although some were bright, and they were more frequently found outside of branchpoints (80.2% of puncta) than within branchpoints (19.8% of puncta). We could detect γ-tubulin-GFP signal in 18% of branchpoints; in approximately half of these branchpoints the γ-tubulin-GFP appeared as puncta, often with multiple puncta per branchpoint, while in the other half of branchpoints the γ-tubulin-GFP signal was spread diffusely through the branchpoint (Fig. 1B). This diffuse signal was similar to that observed when γ-tubulin-GFP is overexpressed[10] (Fig. S1A), although it appeared that the frequency of branchpoint occupancy and the strength of the endogenous γ-tubulin-GFP signal was lower than that observed with ectopically expressed UAS-γ-tubulin-GFP. We noticed that class I neurons display “bubbles”, where the diameter of the dendrite is locally increased to differing extents (Fig. 1A); there were on average 2.6 “bubbles” per 100μm of dendrite with a larger fraction found further from the soma; ~16.5% of

bubbles contained γ-tubulin-GFP signal, either as weak puncta or a diffuse signal (Fig. 1C), and ~36.7% of the γ-tubulin-GFP puncta that we observed within dendrites were found within bubbles. To test whether γ-tubulin-GFP puncta within class I dendrites associate with Golgi outposts, we fixed and stained larval preps expressing γ-tubulin-GFP with the neuronal membrane marker HRP and antibodies against GFP and the Golgi protein GM130. Out of 9 neurons from 3 larvae, we could only find one example where γ-tubulin-GFP colocalised with HRP, and in this case GM130 was also colocalised suggesting it was a Golgi outpost (Fig. 1D). GM130 labels only multi-compartment Golgi outposts[42] but HRP probably labels most, if not all, Golgi outposts; we chose not to use the ectopically expressed Golgi marker ManII-GFP used in previous studies, as we found that this can form puncta, enrichments and long stretches within class I dendrites that are not associated with HRP and thus may not represent genuine Golgi outposts, possibly because an excess of ManII protein causes 'leakage' from Golgi compartments (Fig. S1B). All γ-tubulin-GFP puncta (except for the single occasion noted above), including those within branchpoints, dendrites and bubbles, did not colocalise with HRP or GM130 (Fig. 1E,F). Thus, our data strongly suggests that γ-TuRCs do not typically associate with Golgi outposts within class I neurons, and instead localise to a fraction of branchpoints and dendritic bubbles in a Golgi outpost-independent manner.

For class IV neurons we focussed on the ddaC neuron (hereafter class IV neurons), as these have also been the most widely characterised. We analysed two distinct dendritic regions that we term proximal (within ~100μm of the soma) and distal (over ~200μm from the soma). We detected an average of 2.3 and 0.3 γ-tubulin-GFP puncta per 100μm of dendrite within proximal (10 neurons analysed) and distal (7 neurons analysed) regions, respectively, and the intensity of the majority was only just above background levels, including all of the puncta in the distal regions (Fig. 2A). Nevertheless, we consistently observed bright γ-tubulin-GFP puncta within the primary and secondary branchpoints close to the soma (Fig. 2A). 44.6% of γ-tubulin-GFP puncta observed in the proximal regions were found within the large primary and secondary branchpoints, and 57% of these branchpoints contained γ-tubulin-GFP puncta, which were always relatively bright (Fig. 2A). Staining with HRP and GM130

antibodies showed that these bright γ-tubulin-GFP puncta associated with Golgi outposts (Fig. 2B). Intriguingly, γ-tubulin-GFP only colocalised with HRP puncta that also associated with GM130 (Fig. 2B), suggesting that γ-TuRCs are recruited only to multi-compartment Golgi outposts. The high frequency of proximal branchpoints that contained γ-tubulin-GFP puncta contrasted with the near absence of γ-tubulin-GFP puncta within the smaller branchpoints of the distal arbor, where only 1.7% of these branchpoints contained detectable but very weak γ-tubulin-GFP signal (Fig. 2A insets). In contrast to class I neurons, we found that the vast majority of ectopically expressed ManII-GFP puncta within class IV neurons colocalised with HRP and did not form large accumulations or stretches within the dendrites (Fig. 2C), suggesting that ectopically expressed ManII-GFP can be used as a reliable marker of Golgi outposts in class IV neurons; we observed an average of 11.7 and 5 ManII-GFP-positive Golgi outposts per 100μm of dendrite in within proximal and distal regions, respectively, which is consistent with previous observations[36] and far higher than the frequency of γ-tubulin-GFP puncta that we observed (compare Fig. 2A to Fig. 2C). Thus, only Golgi outposts within the proximal branchpoints of class IV neurons appear to readily associate with γ-TuRCs. In contrast to class I neurons, we very rarely observed γ-tubulin-GFP spread diffusely through branchpoints, suggesting that Golgi outpost-independent recruitment of γ-TuRCs to branchpoints is specific to class I neurons. Moreover, we found far fewer dendritic bubbles per 100μm of dendrite in class IV neurons (0.4 and 0.8 per 100μm dendrite in proximal and distal regions, respectively). Collectively, our data shows that Golgi outposts within class IV neuron branchpoints close to the soma frequently associate with γ-TuRCs, but that the majority of Golgi outposts do not.

γ-tubulin-GFP localises to the somatic Golgi of sensory neurons in a Cnn- and Plp-independent manner

While we could only detect rare γ-tubulin-GFP puncta and enrichments within dendrites, the most striking and obvious localisation of γ-tubulin-GFP within both class I and class IV neurons was as multiple large bright puncta within their soma (Fig. 1A; Fig. 2A; Fig. 3A-C). We also observed similar puncta within the somas of other nearby sensory neurons (Fig. 3A), including external sensory neurons; these sensory neurons

possess basal bodies that appear to associate with large amounts of γ-tubulin-GFP (Fig. 3A). Staining with antibodies against HRP and the GM130, which in mammals localises to the cis-Golgi, showed that all γ-tubulin-GFP puncta within the soma of all sensory neurons associated with somatic Golgi stacks (Fig. 3B,C; Fig. S2), which are typically scattered throughout the cytosol in *Drosophila* cells while still maintaining cis-medial-trans polarity[58]. These Golgi stacks can be oriented either side-on or face-on to the imaging plane, appearing either more elongated or circular, respectively. Our staining showed that the signals of γ-tubulin-GFP and GM130 partially overlapped at side-on stacks, with γ-tubulin-GFP extending further out laterally than GM130 (Fig. 3B; Fig. S2A), suggesting that γ-tubulin-GFP localises on the rims of the cis-Golgi stack. Consistent with this, γ-tubulin-GFP surrounded GM130 in a ring-like pattern on face-on stacks (Fig. 3C; Fig. S2B).

Two proteins, Cnn and Plp, were possible candidates for being responsible for γ-TuRC recruitment to the somatic Golgi, as their homologues are required for proper organisation of microtubules at the somatic Golgi in cycling mammalian cells[24,59–61], and Cnn and Plp have been implicated in γ-TuRC recruitment to Golgi outposts in *Drosophila* class I and class IV neurons, respectively[12,41]. Cnn is a multi-isoform gene with three sets of isoforms driven by three different promotors[62] (Fig. S3A). Promoter one drives the best-studied isoform (that we term Cnn-P1) that localises to centrosomes during mitosis[63–67]; promoter two drives isoforms (Cnn-P2) that are yet to be characterised; and promoter three drives isoforms that are expressed specifically within testes[29] and so have not been considered in this study. Immunostaining with previously-characterised antibodies against Cnn[68] revealed only very weak, if any, signal within the soma of the sensory neurons and few, if any, obvious puncta within their dendrites, although the presumptive basal bodies of the external sensory neurons displayed a strong Cnn signal (data not shown). Given that antibody staining can be problematic, we generated flies where Cnn-P1 or Cnn-P2 were tagged with GFP at their isoform-specific N-termini (hereafter, GFP-Cnn-P1 and GFP-Cnn-P2; Fig. S3A). The GFP insertions appear functional as flies could be kept as homozygous stocks and the localisation of GFP-Cnn-P1 to centrosomes in syncytial embryos was normal (Movie S1). We made flies expressing two genetic copies of the GFP-tagged alleles

and the membrane marker mCD8-RFP specifically within class I da neurons, and imaged living larvae. Under these conditions, we could see only a very weak GFP-Cnn-P1 signal within the soma (Fig. 4A), and staining with HRP and GM130 antibodies and an alexa-488-conjugated anti-GFP "nanobody" showed that only a weak signal of GFP-Cnn-P1 associated with the somatic Golgi sensory neurons (Fig. S3B); the GFP-Cnn-P1 signal at the presumptive basal bodies of the external sensory neurons was very strong (Fig. S3B), but we did not detect GFP-Cnn-P1 associated with HRP puncta within dendrites (Fig. S3B; data not shown). In living larvae, GFP-Cnn-P1 puncta within the dendrites close to the soma were rare (Fig. 4A), but we observed clear GFP-Cnn-P1 accumulations within dendritic bubbles located in the distal regions of the class I arbor (Fig. 4B), similar to the Golgi-independent γ-tubulin-GFP signal that is also found within these dendritic bubbles (Fig. 1C,F). Collectively our data suggests that GFP-Cnn-P1 does not readily associate with Golgi, but accumulates within a fraction of dendritic bubbles, possibly together with γ-tubulin.

In contrast to GFP-Cnn-P1, we did not detect any obvious GFP-Cnn-P2 signal within either soma or dendrites (Fig. S3C). Instead, GFP-Cnn-P2 appeared to be expressed within glia cells that ensheath the axons, soma and part of the proximal dendritic region of the da neurons (Fig. S3C). These Glia are known to help regulate dendritic development[69–71], and thus Cnn-P2 isoforms may have an indirect role in regulating neuronal development by supporting glia function. GFP-Cnn-P2 also localised strongly to the presumptive basal body of external sensory neurons (data not shown). Consistent with the localisation pattern of GFP-Cnn-P1 and GFP-Cnn-P2, γ-tubulin-GFP could still associate with the somatic Golgi in *cnn* mutant larvae, but not to the basal bodies of external sensory neurons (Fig. 4C). We therefore conclude that Cnn is dispensable for γ-TuRC recruitment to the somatic Golgi within sensory neurons.

In contrast to Cnn, antibodies against Plp readily stained the somatic Golgi marked by anti-HRP in all sensory neurons, including class I and class IV da neurons (Fig. S4A). The Plp signal was, however, largely offset from the γ-tubulin-GFP signal at Golgi stacks in both class I and class IV da neurons (Fig. 5A,B), suggesting that they localise to different Golgi compartments. Nevertheless, Plp associated with the HRP- and γ-

tubulin-GFP-positive puncta within branchpoints close to the soma of class IV neurons (Fig. 5C), perhaps because these are multi-compartment Golgi outposts. Plp also associated strongly with the presumptive basal bodies of the external sensory neurons (Fig. S4B), and was enriched within a fraction of the distal dendritic bubbles of the class I arbor (Fig. S4C). Strikingly, γ-tubulin-GFP localisation at the somatic Golgi of all sensory neurons, including class I and class IV neurons, and at proximal Golgi outposts in class IV neurons, were unaffected in *plp* mutant larvae (Fig. 5D), despite the loss of γ-tubulin-GFP at the basal bodies of external sensory cilia (Fig. 5D). This result is consistent with γ-tubulin-GFP and Plp localising to different Golgi compartments (Fig. 5A,B).

In summary, neither Plp nor Cnn are required for the efficient recruitment of γ-TuRCs to the somatic Golgi within sensory neurons, or to the few γ-tubulin-GFP positive Golgi outposts within class IV da neurons.

The Somatic Golgi within da neurons nucleates microtubules

We next wanted to assess whether the somatic Golgi is an active MTOC. We therefore generated flies expressing EB1-GFP and ManII-mCherry within class I da neurons and imaged microtubule growth events (marked by EB1-GFP comets) within the soma with respect to Golgi stacks for a period of up to 5 minutes. We manually tracked each EB1-GFP comet using Image-J and generated overlays such that the origins and paths of each comet could be easily visualised. While some comets originated at locations away from the Golgi, other EB1-GFP comets could be observed emerging from Golgi structures, including occasions where multiple EB1-GFP comets sequentially emerged from a single Golgi structure (Fig. 6A; Movie S2; note that the circle of each track represents the latest position of the EB1 comet).

EB1-GFP marks all microtubule growth events, including both nucleation and microtubule rescue events (where the microtubule regrows after partial depolymerisation). Thus, the origin of EB1-GFP is not a perfect proxy for microtubule nucleation. We therefore used a microtubule regrowth assay where a temperature-control device (CherryTemp, Biotech) was used to rapidly cool samples to 5°C and

then re-heat them to 20°C during continuous imaging of the sample. Cooling leads to the depolymerisation of dynamic microtubules that have not yet been stabilised by post-translational modifications or the binding or microtubule associated proteins. Warming results in microtubule polymerisation, such that depolymerised microtubules will re-grow from their nucleation sites. Moreover, any microtubules that grow a significant amount of time after warming represent new nucleation events. We observed no effect on the distribution of the somatic Golgi stacks during cooling-heating cycles (Fig. 6B; Movie S2), consistent with these stacks not being organised by microtubules from the centrosome. Thermal fluctuations of the glass coverslip caused movements of the sample during the rapid temperature changes, making it difficult to follow the first few timepoints after cooling or warming. Nevertheless, we managed to make movies where the appropriate focal plane was reached shortly after warming and could observe EB1-GFP comets emerging from the ManII-mCherry-labelled Golgi structures (green-labelled comets, Fig. 6B; Movie S2). Some comets emerged from Golgi stacks relatively late after warming (e.g between 50 and 120s post warming), suggesting that nucleation sites are not all "primed" to nucleate at the same time. Moreover, some comets emerged from non-Golgi sites (purple-labelled comets, Fig. 6B; Movie S2), suggesting that either other sites of microtubule nucleation exist or that the comets initially grew from Golgi in a different focal plane. Collectively, our data shows that microtubule nucleation occurs at the somatic Golgi in sensory neurons.

Asymmetric nucleation and Kinesin-2-dependent plus-end-turning and dendritic exclusion help maintain microtubule polarity in axons and dendrites

After finding that the somatic Golgi nucleates microtubules, we next wanted to determine the fate of these microtubules. We imaged class I da neurons expressing EB1-GFP for up to five minutes and followed the path of every visible EB1-GFP comet that emerged from within the soma. We filmed and tracked comets within nine neurons from nine different larvae and collated the data. Overall, ~10 comets originated from within the soma every minute (total of 400 comets in 2405s of imaging), which is similar to the ~9 comets per minute originating from Golgi in RPE1 cells[72], and there did not appear to be a preferential position of origin (Movie S4) i.e. the comets did not

obviously originate closer to the axon or dendrites, consistent with nucleation from multiple well-distributed Golgi stacks. On initial viewing, however, it was obvious that many comets entered the axon, while few entered the dendrites (Fig. 7A; Movie S4). These neurons have a single axon but at least two primary dendrites, but strikingly we found that only 7.1% of comets that initiated within the soma approached the entrance of dendrites, while 34.6% approached the entrance of the axon (Fig. 7C); the remaining 58.2% of comets terminated before reaching either the axon or dendrites.

We reasoned that the preference for comets to approach the axon rather than the dendrites could be due to either a preferential direction of microtubule nucleation or microtubule guidance post nucleation, or both. We observed several occasions where microtubules initially grew at a relatively large angle from the axon but then turned towards it and grew into it (Fig. 7A – see for example time 04:00; Movie S4), suggesting that growing microtubules might be directed along pre-existing microtubules towards the axon. Turning events similar to this have been observed within dendrites, where it has been proposed that the plus-end-directed motor Kinesin-2 associates via its tail with the plus end of a growing microtubule and that Kinesin-2's motor domains simultaneously engage with the shaft of an adjacent microtubule, therefore guiding the plus end of the growing microtubule towards the plus end of the adjacent microtubule[47,49]. Indeed, most turning events within the soma no longer occurred when we knocked down the regulatory subunit of Kinesin-2, Kap3 (Movie S5); comets grew in straight lines unless they collided with the nuclear envelope or cell cortex (although they could still traverse the edge of the cell) (Fig. 7B; Movie S5). Kinesin-2-dependent turning appeared to be important for directing growing microtubules towards the axon, as only 12.9% of comets that originated within the soma approached the entrance of the axon in kap3 RNAi neurons (compared to 34.6% in controls) (Fig. 7C).

Despite these turning events, we also measured the angle of initial EB1-GFP comet growth (i.e. before any turning occurs) by drawing an imaginary line joining the entrance of the axon to the origin of each EB1-GFP comet within control neurons (indicated in Fig. 7A) and plotted the data as a frequency distribution chart (Fig. 7D).

In this way, a comet that initially grows towards the axon would have a very acute angle (e.g. between 0° and 30°), while comets growing away from the axon would have an obtuse angle (between 90° and 180°). We found that there was a strong bias for comets to initially grow with an acute angles (Fig. 7D): 40% of comets grew with an angle less than 30° and 59% of comets grew with an angle less than 60°. In contrast, only 30% of comets grew will an angle above 90°. Thus, as well as kinesin-2-dependent turning events, our data suggests that asymmetric microtubule nucleation from the somatic Golgi helps direct microtubule growth towards the axon.

While directed microtubule nucleation and turning events within the soma appear to contribute to more microtubules entering axons than dendrites, we also noticed that EB1-GFP comets approaching the entrance to a dendrite frequently disappeared in control neurons (Movie S4). Indeed, of the 18 comets that approached the entrance to a dendrite only 4 (22.2%) entered (1.6% of all comets) (Fig. 7E); in contrast, of the 45 comets that approached the entrance to the axon 26 (~57.8%) entered (17.8% of all comets) (Fig. 7E). Thus, growing microtubule ends within the soma appear to be excluded from entering dendrites but not axons. Moreover, of the four comets that entered a dendrite, two appeared to be growing minus ends because they originated from a comet splitting event, where two comets emerge from one and travel in opposite directions (Movie S6). Thus, exclusion of growing microtubules from dendrites may be specific to plus ends. Moreover, EB1-GFP splitting events, which have been observed previously within these neurons[73], suggest that at least some of the microtubules nucleated from the Golgi may be released or severed to allow growth at both ends.

Strikingly, we found that when Kinesin-2 was knocked down many more EB1-GFP comets could enter dendrites. From the four movies of Kap3 RNAi neurons that we made, 50 comets approached the entrance to a dendrite and of these 28 (56%) entered (6.7% of all comets). EB1-GFP comets could also still readily enter axons in Kap3 RNAi neurons: of the 54 comets that approached the entrance to the axon, 43 (~79.6%) entered (10.3% of all comets) (Fig. 7E). The lack of exclusion of EB1-GFP comets from entering dendrites strongly affected microtubule polarity within the proximal region of primary dendrites. When including both comets that grew into

dendrites and comets that originated within dendrites, 80 of 126 comets (63.5%) were anterograde (plus-end-out) in Kap3 RNAi neurons, while only 11 of 146 comets (7.5%) were anterograde in control neurons (Fig. 7F). It is important to note that these comets were observed within the proximal regions of the primary dendrites, prior to any branches, meaning that any anterograde comets must represent microtubules that have grown into the dendrite from the soma and not microtubules that have turned the wrong way at dendritic branchpoints.

A model for asymmetric microtubule nucleation, growth and neurite entry

Based on our observations, we propose a model to help explain how microtubule polarity is maintained within axons and dendrites (Fig. 7G). In this model, γ-TuRCs are localised to the cis-Golgi within the soma and microtubule nucleation events are preferentially directed towards the trans Golgi due to the presence of as yet unidentified proteins at the trans Golgi that stabilise growing microtubule ends, such as CLASP[72]. Cis-medial-trans orientation of Golgi stacks towards the axon would ensure initial growth of microtubules to occur towards the axon. Post microtubule nucleation, Kinesin-2 associates via its tail with the growing plus end and the motor domains engage microtubules that are preferentially oriented with their plus ends pointing towards the axon (due to asymmetric nucleation from the Golgi). This leads to the plus end of the growing microtubule being guided towards along the adjacent microtubule towards the axon. Any microtubules that do happen to grow towards the dendrites are excluded from entering when plus-end-associated kinesin-2 engages with a dendritic microtubule with the opposite polarity. This is because Kinesin-2 would exert a backward force on the growing plus end, presumably leading to plus end stalling and microtubule depolymerisation.

Discussion

Drosophila da neurons are a good *in vivo* model for understanding how neuronal microtubules are regulated, but it has remained unclear how neuronal microtubules are generated and organised. In this paper, we find that the major catalysts of microtubule nucleation, γ-TuRCs, associate with Golgi stacks within the soma of *Drosophila* sensory neurons, including da neurons. We show for the first time that the somatic Golgi is an active MTOC within relatively mature neurons and that this activity generates microtubules destined for the axon. Microtubules within the soma initially grow with a preference towards the axon, suggesting that microtubule nucleation from the somatic Golgi may be asymmetric. Moreover, growing microtubules exhibit Kinesin-2-dependent turning events that help lead growing microtubules towards the axon entry site. As such, many more growing microtubule plus ends reach the axon, rather than the dendrites, and they readily enter. In contrast, microtubules that attempt to grow into dendrites are normally excluded, again in a Kinesin-2-dependent manner. Our data therefore suggests that Kinesin-2 guides growing plus ends within the soma, similar to how it guides microtubule turning events within dendrites[47,49], to help somatic microtubules grow into the axon and to help maintain minus-end-out microtubule polarity within dendrites. Our data also helps to resolve the current controversy regarding whether γ-TuRCs function at Golgi outposts or at dendritic branch points in a Golgi independent manner – we find that both situations exist, but are rarer than previously thought and occur in a neuronal-class-specific and spatially-restricted manner.

While our study shows for the first time that the somatic Golgi generates microtubules within neurons, microtubule nucleation from the somatic Golgi is known to occur in other cell types, including fibroblasts and various types of cultured mammalian cells in interphase[59–61,72,74–76]. Moreover, at least some microtubules nucleated from the somatic Golgi of mammalian cells also grow in a directional manner[72]; this may be particularly important in motile fibroblasts, where Golgi-derived microtubules grow towards the leading edge and may help generate the asymmetric microtubule array required for cell motility[72], and potentially during invasion of cancer cells that establish a polarised pseudopod that is dependent on Golgi-anchored microtubules[59]. Directed

microtubule nucleation likely relies on the inherent polarity of the Golgi stacks. The consensus emerging is that microtubule nucleation occurs at the cis-Golgi due to the recruitment of γ-TuRCs via direct or indirect interactions with cis-Golgi proteins such as GMAP210, AKAP450, Myomegalin and CDK5RAP2 (homologues of Cnn)[24,59,61,75–77]. CLASPs, which localise to the trans-Golgi, are also required for Golgi-derived microtubulesi[72], and it has been suggested that the plus ends of microtubules growing from the cis-Golgi are stabilised by CLASPs at the trans-Golgi and that this dictates a cis-to-trans directionality of microtubule growth from the Golgi[60,78–80]. Whether this occurs in *Drosophila* neurons remains to be explored. *Drosophila* CLASP is known to be a plus-tip protein within axons[81] and is required for axon guidance[82], but to our knowledge a role at the Golgi in any *Drosophila* cell type has not yet been reported.

Intriguingly, the somatic Golgi can "compete" with centrosomes for the ability to organise microtubules[59,76,83]. For example, γ-tubulin can be detected at the Golgi only after depletion of centrosomes in RPE1 cells[59]. This Golgi-centrosome competition could also be true in neurons, as centrosomes are proposed to be inactive in *Drosophila* motor and sensory neurons[39], and the centrosomes in mammalian cultured neurons are active only during early development[30]. An intriguing possibility is that γ-TuRCs are redistributed from centrosomes to the Golgi during neuronal development, as asymmetric nucleation from the Golgi may be necessary for maintaining microtubule polarity within axons and dendrites during later development. Studies in mammalian cultured neurons, however, have not reported γ-TuRC localisation or microtubule nucleation at the somatic Golgi[11,13,14], with one study showing that nucleation within the soma was dependent at least in part on HAUS[11], which mediates the recruitment of γ-TuRCs to pre-formed microtubules. Thus, while γ-tubulin-dependent microtubule nucleation occurs within the soma of cultured mammalian neurons, even up until 21 days *in vitro*[14], it is possible that nucleation from the somatic Golgi is specific to *Drosophila* neurons, although one cannot rule out that microtubules may be nucleated from the somatic Golgi within different types of mammalian neurons or within mammalian neurons *in vivo*.

Our analysis was carried out in third instar larvae where the neurons are fully developed and functional. The axon has already extended and made connections in the central nervous system and the dendritic arbor is established, except for some terminal branches in distal dendrites of class IV neurons that remain dynamic even into late larval stages. It is thus somewhat surprising that microtubules continue to be nucleated within the soma. It is likely that somatic microtubules are necessary for transport of cargos to axonal and dendritic entry sites and it is possible that the somatic microtubule population needs constant renewal. Given that we find Golgi-derived microtubules grow preferentially towards the axon and that somatic Golgi stacks are distributed throughout the soma, it is possible that there is an overall microtubule polarity within the soma itself, with more plus ends pointing towards the axon. Even small biases in the orientation of microtubules within a network can be important for polarised distribution of components, such as in *Drosophila* oocytes[84], so it is possible that a similar bias within neuronal soma is important for directing molecules into axons and dendrites. Alternatively, or in conjunction with this, the Golgi-derived microtubules that continually grow into axons may be necessary to support axonal function throughout the lifetime of the neuron, possibly because of damage caused to axonal microtubules during motor-driven cargo transport[85].

If there is an asymmetric microtubule network within the soma, it may also be important for guiding growing microtubules towards the axon, rather than towards the dendrites. We have shown that Kinesin-2 mediates turning events within the soma that increase the proportion of growing microtubules reaching the axon entry site. The plus-end-directed motor Kinesin-2 is thought to associate via its tail region with growing plus ends due to an interaction with APC, which itself binds to EB1[49]. *In vitro* experiments have shown that Kinesin-2 can guide microtubule plus ends along adjacent microtubule when Kinesin-2 is artificially tethered to the plus end[86,87], and this guidance mechanism appears to be true at dendritic branchpoints *in vivo* where Kinesin-2 is necessary for microtubules to turn towards the soma[47,49]. APC-2 is believed to recruit APC to branchpoints where it can function in plus end turning[47], but APC-2 also accumulates with the soma of class I neurons[47,49]. We therefore think that a similar mechanism works in the soma, where plus-end-associated Kinesin-2 directs

growing microtubules towards the axon along an asymmetric microtubule network (with more plus ends pointing towards the axon) that has been established by asymmetric nucleation from the somatic Golgi. Moreover, the role of Kinesin-2 at plus ends is not specific to turning events. We find that Kinesin-2 is necessary for the exclusion of growing plus ends from entering dendrites. Presumably, plus-end-associated Kinesin-2 exerts a backward force on growing microtubules when they grow close enough to a microtubule with opposite polarity, such is the case when somatic microtubules attempt to grow into dendrites (Fig. 7G). While it is already known that Kinesin-2 is necessary for maintaining minus-end-out polarity within dendrites[47,49], these previous studies assessed polarity within dendrites further from the soma. Our analysis is different in that we have assessed microtubule polarity in the proximal region of the primary dendrite, before any dendritic branches. Thus, the large fraction of microtubules that display plus-end-out polarity after Kinesin-2 RNAi within the proximal dendrite cannot originate from microtubules that turn the wrong way at dendritic branchpoints; the reversal of polarity within this region is produced purely from microtubules growing into the dendrites from the soma.

Until this present study, it had remained unclear where γ-TuRCs were localised within *Drosophila* da neurons. Golgi outposts within the dendrites have been proposed as sites of γ-TuRC recruitment and microtubule nucleation[12,41,42], but these studies did not examine the *in vivo* localisation of γ-TuRCs. Another study questioned the role of Golgi outposts in microtubule nucleation by showing that ectopically expressed γ-tubulin-GFP is concentrated within dendritic branchpoints independent of Golgi outposts[39]. In this study, we used endogenously tagged γ-tubulin-GFP, and we only analysed cells expressing two genetic copies (which is necessary due to the lower expression levels of endogenously regulated proteins compared to genes driven from ectopic promotors). From our analysis, we conclude that only Golgi outposts located within the proximal branchpoints of class IV neurons readily associate with γ-TuRCs. The γ-tubulin-GFP signal at these Golgi outposts was relatively bright and easy to detect, proving that accumulations of γ-tubulin-GFP can be detected away from centrosomes. We did not detect any bright γ-tubulin-GFP puncta within any other regions of the class IV arbor, and any weak puncta were far less numerous than HRP

puncta and ManII-mCherry puncta. Collectively, this suggests that the vast majority of Golgi outposts within class IV neurons lack γ-TuRCs.

The situation within class I da neurons dendrites is both similar and different. We only observed one occasion from 9 neurons where a Golgi outpost had detectable γ-tubulin-GFP signal. Instead, we found that γ-tubulin-GFP accumulated within a fraction of dendritic branchpoints and dendritic bubbles in a Golgi-independent manner. The accumulation in branchpoints resembles that observed when γ-tubulin-GFP is over-expressed, but we stress that endogenous γ-tubulin-GFP accumulations within branchpoints are less numerous, weaker, and occur in class I but not class IV da neurons.

While our data suggests that most Golgi outposts do not recruit γ-TuRCs, we cannot rule out that Golgi outposts recruit undetectable numbers of γ-TuRCs that are sufficient for microtubule nucleation. We also cannot rule out that Golgi outposts regulate microtubule formation or growth in a γ-TuRC-independent manner. Recent studies have highlighted the role of TOG and TPX2 protein families in microtubule nucleation[88] and these proteins can promote microtubule nucleation *in vitro* in the absence of γ-TuRCs[89,90]. Indeed, depletion of the *Drosophila* TOG domain protein, Msps, strongly reduces EB1-comets within da neuron dendrites[91]. Structures such as Golgi outposts may also sequester and stabilise severed microtubules and then help control their subsequent polymerisation. We can rule out, however, a role for Plp and Cnn in recruiting γ-TuRCs to Golgi, including both somatic Golgi and Golgi outposts. While Plp associates with both the somatic Golgi and Golgi outposts, Plp localises primarily to a different Golgi compartment than γ-tubulin-GFP and γ-tubulin-GFP remains associated with the somatic Golgi and proximal Golgi outposts within *plp* mutant class IV neurons. γ-tubulin-GFP also remains associated with the somatic Golgi in *cnn* mutants and endogenous Cnn localises to dendritic bubbles rather than to Golgi outposts. It will therefore be interesting to investigate whether the dendritic arborisation defects observed in *cnn* mutant class I da neurons[41] and *plp* mutant class IV da neurons[12] are at least partly due to non-cell-autonomous defects. With this in

mind, it is interesting that we have found that the previously uncharacterised Cnn-P2 isoform is expressed strongly within the Glial cells that ensheath the da neurons.

In summary, our data shows that that microtubules are nucleated from the somatic Golgi within *Drosophila* sensory neurons and that Kinesin-2 mediates directional microtubule growth towards the axon and exclusion of growing microtubules from entering dendrites. These processes help supply microtubules into axons and maintain minus-end-out microtubule polarity within dendrites, respectively. Our data regarding class I – specific dendritic bubbles enriched with potential microtubule regulators also suggests that microtubule formation is controlled differently in different classes of neurons, which could in theory lead to different dendritic branching patterns.

Acknowledgements

This work was supported by a Wellcome Trust and Royal Society Sir Henry Dale Fellowship (105653/Z/14/Z) and an Isaac Newton Trust Research grant (18.23(p)) awarded to PTC, and an Association pour la Recherche sur le Cancer grant (PJA 20181208148) awarded to AG. We thank Matt Wayland for help with confocal microscopy and members of the Conduit lab for critical reading of the manuscript. The work benefited from use of the Imaging Facility, Department of Zoology, supported by a Sir Isaac Newton Trust Research Grant (18.07ii(c)).

Author Contributions

PTC and AM designed the study, analysed data and wrote the manuscript. AM performed the vast majority of experiments; PB imaged and quantified the frequency of Golgi outposts within class I and class IV da neurons; PTC performed some of the EB1-GFP comet imaging. FB and AG supplied the γ-tubulin-ssss-eGFP fly line.

Declaration of Interests

The authors declare no competing interests.

References

1. Goodson, H. V. & Jonasson, E. M. Microtubules and Microtubule-Associated Proteins. *Csh Perspect Biol* **10**, a022608 (2018).

2. Kelliher, M. T., Saunders, H. A. & Wildonger, J. Microtubule control of functional architecture in neurons. *Curr Opin Neurobiol* **57**, 39–45 (2019).

3. Tas, R. P. *et al.* Differentiation between Oppositely Oriented Microtubules Controls Polarized Neuronal Transport. *Neuron* **96**, 1264-1271.e5 (2017).

4. Kapitein, L. C. & Hoogenraad, C. C. Building the Neuronal Microtubule Cytoskeleton. *Neuron* **87**, 492 506 (2015).

5. Harterink, M. *et al.* Local microtubule organization promotes cargo transport in C. elegans dendrites. *J Cell Sci* **131**, jcs.223107 (2018).

6. Tovey, C. A. & Conduit, P. T. Microtubule nucleation by γ-tubulin complexes and beyond. *Essays Biochem* **91**, EBC20180028 (2018).

7. Kollman, J. M., Merdes, A., Mourey, L. & Agard, D. A. Microtubule nucleation by γ-tubulin complexes. *Nat Rev Mol Cell Bio* **12**, 709 721 (2011).

8. Wieczorek, M. *et al.* Asymmetric molecular architecture of the human γ-tubulin ring complex. *Biorxiv* 820142 (2019) doi:10.1101/820142 .

9. Kollman, J. M., Polka, J. K., Zelter, A., Davis, T. N. & Agard, D. A. Microtubule nucleating gamma-TuSC assembles structures with 13-fold microtubule-like symmetry. *Nature* **466**, 879 882 (2010).

10. Nguyen, M. M. *et al.* γ-Tubulin controls neuronal microtubule polarity independently of Golgi outposts. *Mol Biol Cell* **25**, 2039–2050 (2014).

11. Sánchez-Huertas, C. *et al.* Non-centrosomal nucleation mediated by augmin organizes microtubules in post-mitotic neurons and controls axonal microtubule polarity. *Nat Commun* **7**, 12187 (2016).

12. Ori-McKenney, K. M., Jan, L. & Jan, Y.-N. Golgi outposts shape dendrite morphology by functioning as sites of acentrosomal microtubule nucleation in neurons. *Neuron* **76**, 921 930 (2012).

13. Yamada, M. & Hayashi, K. Microtubule nucleation in the cytoplasm of developing cortical neurons and its regulation by brain-derived neurotrophic factor. *Cytoskeleton* **76**, 339–345 (2019).

14. Yau, K. *et al.* Microtubule Minus-End Binding Protein CAMSAP2 Controls Axon Specification and Dendrite Development. *Neuron* **82**, 1058 1073 (2014).

15. Mitani, T. *et al.* Bi-allelic Pathogenic Variants in TUBGCP2 Cause Microcephaly and Lissencephaly Spectrum Disorders. *Am J Hum Genetics* (2019) doi:10.1016/j.ajhg.2019.09.017 .

16. Poirier, K. *et al.* Mutations in TUBG1, DYNC1H1, KIF5C and KIF2A cause malformations of cortical development and microcephaly. *Nat Genet* **45**, 639 647 (2013).

17. Bahi-Buisson, N. *et al.* The wide spectrum of tubulinopathies: what are the key features for the diagnosis? *Brain* **137**, 1676–1700 (2014).

18. Sanchez, A. D. & Feldman, J. L. Microtubule-organizing centers: from the centrosome to non-centrosomal sites. *Curr Opin Cell Biol* **44**, 93 101 (2016).

19. Meunier, S. & Vernos, I. Acentrosomal Microtubule Assembly in Mitosis: The Where, When, and How. *Trends Cell Biol* **26**, 80 87 (2016).

20. Teixidó-Travesa, N., Roig, J. & Lüders, J. The where, when and how of microtubule nucleation - one ring to rule them all. *J Cell Sci* **125**, 4445 4456 (2012).

21. Farache, D., Emorine, L., Haren, L. & Merdes, A. Assembly and regulation of γ-tubulin complexes. *Open Biol* **8**, 170266 (2018).

22. Lin, T., Neuner, A. & Schiebel, E. Targeting of γ-tubulin complexes to microtubule organizing centers: conservation and divergence. *Trends Cell Biol* **25**, 296 307 (2014).

23. Conduit, P. T. *et al.* A molecular mechanism of mitotic centrosome assembly in Drosophila. *Elife* **3**, 2987 (2014).

24. Wang, Z. *et al.* Conserved Motif of CDK5RAP2 Mediates Its Localization to Centrosomes and the Golgi Complex. *J Biol Chem* **285**, 22658–22665 (2010).

25. Zhang, J. & Megraw, T. L. Proper recruitment of gamma-tubulin and D-TACC/Msps to embryonic Drosophila centrosomes requires Centrosomin Motif 1. *Mol Biol Cell* **18**, 4037 4049 (2007).

26. Haren, L., Stearns, T. & Lüders, J. Plk1-dependent recruitment of gamma-tubulin complexes to mitotic centrosomes involves multiple PCM components. *Plos One* **4**, e5976 (2009).

27. Muroyama, A., Seldin, L. & Lechler, T. Divergent regulation of functionally distinct γ-tubulin complexes during differentiation. *J Cell Biology* **213**, 679–692 (2016).

28. Choi, Y.-K., Liu, P., Sze, S., Dai, C. & Qi, R. Z. CDK5RAP2 stimulates microtubule nucleation by the γ-tubulin ring complex. *J Cell Biology* **191**, 1089–1095 (2010).

29. Chen, J. V., Buchwalter, R. A., Kao, L.-R. & Megraw, T. L. A Splice Variant of Centrosomin Converts Mitochondria to Microtubule-Organizing Centers. *Curr Biol* **27**, 1928 1940.e6 (2017).

30. Stiess, M. *et al.* Axon Extension Occurs Independently of Centrosomal Microtubule Nucleation. *Science* **327**, 704–707 (2010).

31. Baas, P. W., Karabay, A. & Qiang, L. Microtubules cut and run. *Trends Cell Biol* **15**, 518 524 (2005).

32. Lu, W., Fox, P., Lakonishok, M., Davidson, M. W. & Gelfand, V. I. Initial neurite outgrowth in Drosophila neurons is driven by kinesin-powered microtubule sliding. *Curr Biol* **23**, 1018 1023 (2013).

33. del Castillo, U., Lu, W., Winding, M., Lakonishok, M. & Gelfand, V. I. Pavarotti/MKLP1 Regulates Microtubule Sliding and Neurite Outgrowth in Drosophila Neurons. *Curr Biol* **25**, 1 6 (2014).

34. Rao, A. N. *et al.* Cytoplasmic Dynein Transports Axonal Microtubules in a Polarity-Sorting Manner. *Cell Reports* **19**, 2210–2219 (2017).

35. Klinman, E., Tokito, M. & Holzbaur, E. L. CDK5-dependent activation of dynein in the axon initial segment regulates polarized cargo transport in neurons. *Traffic* **18**, 808–824 (2017).

36. Zheng, Y. *et al.* Dynein is required for polarized dendritic transport and uniform microtubule orientation in axons. *Nat Cell Biol* **10**, 1172 1180 (2008).

37. del Castillo, U., Winding, M., Lu, W. & Gelfand, V. I. Interplay between kinesin-1 and cortical dynein during axonal outgrowth and microtubule organization in Drosophila neurons. *Elife* **4**, e10140 (2015).

38. Yan, J. *et al.* Kinesin-1 regulates dendrite microtubule polarity in Caenorhabditis elegans. *Elife* **2**, e00133 (2013).

39. Nguyen, M. M., Stone, M. C. & Rolls, M. M. Microtubules are organized independently of the centrosome in Drosophila neurons. *Neural Dev* **6**, 38 (2011).

40. Cunha-Ferreira, I. *et al.* The HAUS Complex Is a Key Regulator of Non-centrosomal Microtubule Organization during Neuronal Development. *Cell Reports* **24**, 791 800 (2018).

41. Yalgin, C. *et al.* Centrosomin represses dendrite branching by orienting microtubule nucleation. *Nat Neurosci* **18**, 1437 1445 (2015).

42. Zhou, W. *et al.* GM130 is required for compartmental organization of dendritic golgi outposts. *Curr Biol* **24**, 1227 1233 (2014).

43. Grueber, W. B., Jan, L. Y. & Jan, Y.-N. Tiling of the Drosophila epidermis by multidendritic sensory neurons. *Development (Cambridge, England)* **129**, 2867 2878 (2002).

44. Hill, S. E. *et al.* Development of dendrite polarity in Drosophila neurons. *Neural Dev* **7**, 34 (2012).

45. Stone, M. C., Roegiers, F. & Rolls, M. M. Microtubules have opposite orientation in axons and dendrites of Drosophila neurons. *Mol Biol Cell* **19**, 4122 4129 (2008).

46. Sears, J. C. & Broihier, H. T. FoxO regulates microtubule dynamics and polarity to promote dendrite branching in Drosophila sensory neurons. *Dev Biol* **418**, 40 54 (2016).

47. Weiner, A. T., Lanz, M. C., Goetschius, D. J., Hancock, W. O. & Rolls, M. M. Kinesin-2 and Apc function at dendrite branch points to resolve microtubule collisions. *Cytoskeleton* **73**, 35–44 (2016).

48. Rolls, M. M. & Jegla, T. J. Neuronal polarity: an evolutionary perspective. *J Exp Biology* **218**, 572–580 (2015).

49. Mattie, F. J. *et al.* Directed microtubule growth, +TIPs, and kinesin-2 are required for uniform microtubule polarity in dendrites. *Curr Biol* **20**, 2169 2177 (2010).

50. Gardiol, A., Racca, C. & Triller, A. Dendritic and Postsynaptic Protein Synthetic Machinery. *J Neurosci* **19**, 168–179 (1999).

51. Horton, A. C. & Ehlers, M. D. Dual Modes of Endoplasmic Reticulum-to-Golgi Transport in Dendrites Revealed by Live-Cell Imaging. *J Neurosci* **23**, 6188–6199 (2003).

52. Pierce, J., van Leyen, K. & McCarthy, J. Translocation machinery for synthesis of integral membrane and secretory proteins in dendritic spines. *Nat Neurosci* **3**, nn0400_311 (2000).

53. Pierce, J. P., Mayer, T. & McCarthy, J. B. Evidence for a satellite secretory pathway in neuronal dendritic spines. *Curr Biol* **11**, 351–355 (2001).

54. Ye, B. *et al.* Growing Dendrites and Axons Differ in Their Reliance on the Secretory Pathway. *Cell* **130**, 717–729 (2007).

55. Horton, A. C. *et al.* Polarized Secretory Trafficking Directs Cargo for Asymmetric Dendrite Growth and Morphogenesis. *Neuron* **48**, 757–771 (2005).

56. Nakamura, N. *et al.* Characterization of a cis-Golgi matrix protein, GM130. *J Cell Biology* **131**, 1715–1726 (1995).

57. Kondylis, V. & Rabouille, C. The Golgi apparatus: Lessons from Drosophila.

Febs Lett **583**, 3827–3838 (2009).

58. Tovey, C. A. *et al.* γ-TuRC Heterogeneity Revealed by Analysis of Mozart1. *Curr Biol* **28**, 2314 2323.e6 (2018).

59. Wu, J. *et al.* Molecular Pathway of Microtubule Organization at the Golgi Apparatus. *Dev Cell* **39**, 44 60 (2016).

60. Rios, R. The centrosome-Golgi apparatus nexus. *Philosophical Transactions Royal Soc B Biological Sci* **369**, 20130462–20130462 (2014).

61. Roubin, R. *et al.* Myomegalin is necessary for the formation of centrosomal and Golgi-derived microtubules. *Biol Open* **2**, 238 250 (2013).

62. Eisman, R. C., Phelps, M. A. & Kaufman, T. C. Centrosomin: a complex mix of long and short isoforms is required for centrosome function during early development in Drosophila melanogaster. *Genetics* **182**, 979 997 (2009).

63. Megraw, T., Li, K., Kao, L. & Kaufman, T. The centrosomin protein is required for centrosome assembly and function during cleavage in Drosophila. *Development (Cambridge, England)* **126**, 2829 2839 (1999).

64. Lucas, E. P. & Raff, J. W. Maintaining the proper connection between the centrioles and the pericentriolar matrix requires Drosophila Centrosomin. *J Cell Biology* **178**, 725–732 (2007).

65. Conduit, P. T. *et al.* The centrosome-specific phosphorylation of Cnn by Polo/Plk1 drives Cnn scaffold assembly and centrosome maturation. *Dev Cell* **28**, 659 669 (2014).

66. Fu, J. & Glover, D. M. Structured illumination of the interface between centriole and peri-centriolar material. *Open Biol* **2**, 120104 (2012).

67. Mennella, V., Agard, D. A., Huang, B. & Pelletier, L. Amorphous no more: subdiffraction view of the pericentriolar material architecture. *Trends Cell Biol* **24**, 188 197 (2013).

68. Dobbelaere, J. *et al.* A genome-wide RNAi screen to dissect centriole duplication and centrosome maturation in Drosophila. *Plos Biol* **6**, e224 (2008).

69. Yadav, S. *et al.* Glial ensheathment of the somatodendritic compartment regulates sensory neuron structure and activity. *Proc National Acad Sci* **116**, 201814456 (2019).

70. Sepp, K. J. & Auld, V. J. Reciprocal Interactions between Neurons and Glia Are Required for Drosophila Peripheral Nervous System Development. *J Neurosci* **23**, 8221–8230 (2003).

71. Han, C., Jan, L. & Jan, Y.-N. Enhancer-driven membrane markers for analysis of nonautonomous mechanisms reveal neuron–glia interactions in Drosophila. *Proc National Acad Sci* **108**, 9673–9678 (2011).

72. Efimov, A. *et al.* Asymmetric CLASP-dependent nucleation of noncentrosomal microtubules at the trans-Golgi network. *Dev Cell* **12**, 917 930 (2007).

73. Feng, C. *et al.* Patronin-mediated minus end growth is required for dendritic microtubule polarity. *J Cell Biology* **218**, 2309–2328 (2019).

74. Chabin-Brion, K. *et al.* The Golgi Complex Is a Microtubule-organizing Organelle. *Mol Biol Cell* **12**, 2047–2060 (2001).

75. Rivero, S., Cardenas, J., Bornens, M. & Rios, R. M. Microtubule nucleation at the cis-side of the Golgi apparatus requires AKAP450 and GM130. *Embo J* **28**, 1016 1028 (2009).

76. Rí́os, R. M., Sanchí́s, A., Tassin, A., Fedriani, C. & Bornens, M. GMAP-210 Recruits γ-Tubulin Complexes to cis-Golgi Membranes and Is Required for Golgi Ribbon Formation. *Cell* **118**, 323–335 (2004).

77. Hurtado, L. *et al.* Disconnecting the Golgi ribbon from the centrosome prevents directional cell migration and ciliogenesis. *J Cell Biology* **193**, 917–933 (2011).

78. Vinogradova, T., Miller, P. M. & Kaverina, I. Microtubule network asymmetry in motile cells: role of Golgi-derived array. *Cell Cycle* **8**, 2168 2174 (2009).

79. Sütterlin, C. & Colanzi, A. The Golgi and the centrosome: building a functional partnership. *J Cell Biology* **188**, 621–628 (2010).

80. Zhu, X. & Kaverina, I. Golgi as an MTOC: making microtubules for its own good. *Histochem Cell Biol* **140**, 361–367 (2013).

81. Beaven, R. *et al.* Drosophila CLIP-190 and mammalian CLIP-170 display reduced microtubule plus end association in the nervous system. *Mol Biol Cell* **26**, 1491–1508 (2015).

82. Lee, H. *et al.* The Microtubule Plus End Tracking Protein Orbit/MAST/CLASP Acts Downstream of the Tyrosine Kinase Abl in Mediating Axon Guidance. *Neuron* **42**, 913–926 (2004).

83. Gavilan, M. P. *et al.* The dual role of the centrosome in organizing the microtubule network in interphase. *Embo Rep* **19**, e45942 (2018).

84. Zimyanin, V. L. *et al.* In vivo imaging of oskar mRNA transport reveals the mechanism of posterior localization. *Cell* **134**, 843 853 (2008).

85. Triclin, S. *et al.* Self-repair protects microtubules from their destruction by

molecular motors. *Biorxiv* 499020 (2018) doi:10.1101/499020 .

86. Chen, Y., Rolls, M. M. & Hancock, W. O. An EB1-Kinesin Complex Is Sufficient to Steer Microtubule Growth In Vitro. *Curr Biol* **24**, 316–321 (2014).

87. Doodhi, H., Katrukha, E. A., Kapitein, L. C. & Akhmanova, A. Mechanical and Geometrical Constraints Control Kinesin-Based Microtubule Guidance. *Curr Biol* **24**, 322–328 (2014).

88. Roostalu, J. & Surrey, T. Microtubule nucleation: beyond the template. *Nat Rev Mol Cell Bio* **91**, 321 710 (2017).

89. Roostalu, J., Cade, N. I. & Surrey, T. Complementary activities of TPX2 and chTOG constitute an efficient importin-regulated microtubule?nucleation module. *Nat Cell Biol* **17**, 1422 1434 (2015).

90. Woodruff, J. B. *et al.* The Centrosome Is a Selective Condensate that Nucleates Microtubules by Concentrating Tubulin. *Cell* **169**, 1066 1077.e10 (2017).

91. Stone, M. C., Nguyen, M. M., Tao, J., Allender, D. L. & Rolls, M. M. Global up-regulation of microtubule dynamics and polarity reversal during regeneration of an axon from a dendrite. *Mol Biol Cell* **21**, 767 777 (2010).

92. Martinez-Campos, M., Basto, R., Baker, J., Kernan, M. & Raff, J. W. The Drosophila pericentrin-like protein is essential for cilia/flagella function, but appears to be dispensable for mitosis. *J Cell Biology* **165**, 673–683 (2004).

93. Broadie, K. & Bate, M. Activity-dependent development of the neuromuscular synapse during drosophila embryogenesis. *Neuron* **11**, 607–619 (1993).

Figure legends

Figure 1

Endogenously-tagged γ-tubulin-GFP localises to a fraction of branchpoints and dendritic bubbles within class I da neurons. (**A**) Fluorescent confocal images of the proximal region of a class I da neurons expressing 221-gal4>UAS-mCD8-RFP (greyscale) within a living 3rd instar larvae expressing two copies of endogenously-tagged γ-tubulin-GFP (green). Left panel (A) shows an overlay of the GFP and RFP signals, right panel (A') shows only the GFP signal with the outline of the neuron drawn for convenience; white, blue and orange arrowheads indicate γ-tubulin-GFP puncta or accumulations within dendritic stretches, branchpoints and dendritic bubbles, respectively. (**B,C**) Selected images of γ-tubulin-GFP-positive branchpoints (B) or dendritic bubbles (C) from different class I da neurons within living 3rd instar larvae expressing 221-gal4>UAS-mCD8-RFP and γ-tubulin-GFP, as in (A), highlighting the variability in γ-tubulin-GFP signal within branchpoints and dendritic bubbles. (**D-F**) Confocal images show branchpoints (D,E) or dendritic bubbles (F) from 3rd instar larvae expressing endogenous γ-tubulin-GFP fixed and immunostained with antibodies against GFP (green), GM130 (magenta) and HRP (greyscale). γ-tubulin-GFP signal within dendrites was only once observed co-localising with GM130 and HRP signal (D), with all other occasions indicating Golgi-independent localisation at both branchpoints (E) and dendritic bubbles (F). See also Figure S1.

Figure 2

Endogenously-tagged γ-tubulin-GFP localises to a small fraction of proximal Golgi outposts within class IV da neurons. (**A**) Fluorescent confocal images of the proximal region of a class IV da neurons expressing ppk-gal4>UAS-mCD8-RFP (greyscale) within a living 3rd instar larvae expressing two copies of endogenously-tagged γ-tubulin-GFP (green). Left panel (A) shows an overlay of the GFP and RFP signals, right panel (A') shows only the GFP signal with the outline of the neuron drawn for convenience; insets show examples of distal dendrites located far from the soma; white and yellow arrowheads indicate bright or weak γ-tubulin-GFP puncta within proximal or distal dendrites, respectively. (**B**) Images show a γ-tubulin-GFP-positive

proximal branchpoint from a 3rd instar larva expressing endogenous γ-tubulin-GFP fixed and immunostained with antibodies against GFP (green), GM130 (magenta) and HRP (greyscale). Stars indicate GM130 foci from overlapping epidermal cells. Arrowhead indicates a γ-tubulin-GFP-positive Golgi outpost that contains both GM130 and HRP signal; these types of Golgi outposts were frequently observed within proximal class IV branchpoints. Other HRP puncta do not co-localise with GM130 or γ-tubulin-GFP, suggesting that only GM130-positive Golgi outposts recruit γ-TuRCs. (**C**) Confocal images show the proximal region of a class IV dendritic arbor within a 3rd instar larva expressing ppk-gal4>UAS-ManII-GFP (to mark medial Golgi) fixed and immunostained with antibodies against GFP (fire) and HRP (greyscale within insets). HRP staining is shown within insets for regions of the arbor that contain ManII-GFP puncta – note how each ManII-GFP puncta colocalises with an HRP puncta, indicating that ectopically expressed ManII-GFP can be used as a reliable Golgi outpost marker within class IV neurons (this is not true of class I neurons – see Figure S1B).

Figure 3

Endogenously-tagged γ-tubulin-GFP localises to the somatic Golgi of sensory neurons. (**A**) Confocal images show the somas and some proximal dendrites of sensory neurons within the dorsal cluster, including class I (yellow), class IV (blue), external sensory (pink) and other unidentified neurons (orange) from a 3rd instar larva expressing two copies of endogenously-tagged γ-tubulin-GFP and immunostained with antibodies against GFP (green) and HRP (greyscale). Upper panel (A) shows an overlay of the GFP and HRP signals, lower panel (A') shows only the GFP signal with coloured outlines of the different neurons drawn for convenience. HRP staining marks the multiple well-distributed Golgi stacks within the soma of each neuron and co-localises with γ-tubulin-GFP signal. (**B, C**) Confocal images show the soma of class I (B) or class IV (C) da neurons from a 3rd instar larva expressing two copies of endogenous γ-tubulin-GFP fixed and immunostained with antibodies against GFP (green), GM130 (magenta) and HRP (greyscale). γ-tubulin-GFP and GM130 signals associate at presumptive side-on stacks (enlarged boxes in (B)) and end-on stacks (enlarged boxes in (C)) in a way that suggests γ-TuRCs are recruited to the rims of the cis-Golgi. See also Figure S2.

Figure 4

Cnn-P1 localises to dendritic bubbles within class I da neurons and is dispensable for γ-tubulin-GFP recruitment to the somatic Golgi. (**A,B**) Fluorescent confocal images of proximal (A) and distal (B) regions of class I da neurons expressing 221-gal4>UAS-mCD8-RFP (greyscale) within a living 3rd instar larvae expressing two copies of endogenously-tagged GFP-Cnn-P1 (green). Upper panels show an overlay of the GFP and RFP channels, lower panels show only the GFP channel with the outline of the neurons drawn for convenience. Arrowhead in (A) indicates a rare dendritic GFP-Cnn-P1 puncta within a proximal dendritic bubble, while arrowheads in (B) indicate more frequent GFP-Cnn-P1 accumulations within distal dendritic bubbles. (**C**) Confocal images show the somas and some proximal dendrites of sensory neurons within the dorsal cluster from a 3rd instar *cnn* mutant larva expressing two copies of endogenously-tagged γ-tubulin-GFP and immunostained with antibodies against GFP (green), HRP (greyscale) and Cnn (magenta). HRP staining marks the multiple well-distributed Golgi stacks within the neuronal soma of each neuron and co-localises with γ-tubulin-GFP within the class I da neuron soma of these *cnn* mutant larvae, as indicated in (C'). HRP staining also appears to mark the presumptive basal bodies of external sensory neurons (see also Figure 3), which within these *cnn* mutants lacks both Cnn and γ-tubulin-GFP signal, as indicated in (C''). See also Figure S3.

Figure 5

Endogenous Plp localises to Golgi but is dispensable for γ-tubulin-GFP recruitment to both somatic Golgi and Golgi outposts. (**A-C**) Confocal images show the soma of class I (A) or class IV (B) da neurons and a proximal branchpoint of a class IV neuron (C) from 3rd instar larvae expressing two copies of endogenous γ-tubulin-GFP fixed and immunostained with antibodies against GFP (green), Plp (magenta) and HRP (greyscale). γ-tubulin-GFP and Plp signals associate with Golgi stacks within the soma of both class I (B) and class IV (C) neurons but are slightly offset, indicating that γ-TuRCs and Plp localise to different Golgi compartments. This can be best seen in the enlarged images of Golgi stacks on the right of (A) and (B).

Arrowhead in (C) indicates a γ-tubulin-GFP-positive Golgi outpost that contains both Plp and HRP signal; these types of Golgi outposts were frequently observed within proximal class IV branchpoints. (**D**) Confocal images show the somas and some proximal dendrites of sensory neurons within the dorsal cluster, including class I (yellow), class IV (blue), external sensory (pink) and other neurons within the dorsal cluster (orange) from a *plp* mutant 3rd instar larva expressing two copies of endogenously-tagged γ-tubulin-GFP and immunostained with antibodies against GFP (green), HRP (greyscale) and GM130 (magenta). Left panel (D) shows an overlay of the GFP and HRP signal, with insets showing overlays of γ-tubulin-GFP and GM130 for the class I soma (yellow box) and class IV soma (blue box); right panel (D') shows the GFP channel with coloured outlines of the different neurons drawn for convenience, with insets showing the γ-tubulin-GFP, HRP and GM130 signals from a class IV proximal branchpoint. Note how γ-tubulin-GFP is still strongly associated with the somatic Golgi and proximal Golgi outpost, but not the basal bodies of external sensory neurons, in these *plp* mutants. See also Figure S4.

Figure 6

Somatic Golgi stacks nucleate microtubules. (**A,B**) Widefield fluorescent images from movies showing the somas of class I da neurons expressing 221-gal4>UAS-EB1-GFP (greyscale) and 221-gal4>UAS-ManII-mCherry (magenta). Each EB1-GFP comet was manually tracked in image J and the tracks were drawn over each image, with the last location of the EB1-GFP comet indicated by a filled circle. The arrow in (A) indicates a Golgi stack where sequential EB1-GFP comets emerge during the movie. The sample in (B) was subjected to a warm-cool-warm temperature cycle to induce depolymerisation of dynamic microtubules (5˚C) for 3 minutes and then microtubule polymerisation (20˚C), revealing sites of microtubule nucleation. Tracks in (A) are drawn in default multi-colour, while tracks in (B) are manually colour coded to indicate comets that emerged from Golgi stacks (green) and those that emerged from elsewhere (purple). Time in min:s from either the start of the movie (A) or from the 5˚C to 20˚C transition (B) is shown in the top right of each image. EB1-GFP comets emerge from multiple Golgi stacks both during normal imaging (A) and during microtubule polymerisation after warming (B). Note how some microtubules emerge from Golgi

stacks over a minute after warming, showing that these are newly nucleated microtubules. See also Movie S2 and Movie S3.

Figure 7

Microtubules within the soma grow preferentially towards the axon and are excluded from entering dendrites in a Kinesin-2-dependent manner. (**A,B**) Widefield fluorescent images from movies showing the somas of class I da neurons expressing either 221-gal4>UAS-EB1-GFP alone (control) or 221-gal4>UAS-EB1-GFP and 221-gal4>UAS-Kap3 RNAi (Kinesin-2 RNAi). Each EB1-GFP comet (greyscale) was manually tracked in image J and the tracks are drawn in default multi-colour over each image, with the last location of the EB1-GFP comet indicated by a filled circle. Time in min:s from the start of the movie is shown in the bottom right of each image. In control neurons (A), EB1-GFP comets can turn within the soma and readily grow into axons but not dendrites. In Kinesin-2 RNAi neurons (B), comets fail to turn within the soma unless they encounter the nuclear envelope or cell cortex, and comets can readily grow into both axons and dendrites. (**C**) Graph shows the % of comets that approach either the axon (green) or the dendrites (magenta) in either control (left) or Kinesin-2 RNAi (right) class I da neuron soma. (**D**) Graph shows a frequency distribution of the initial angle of EB1-GFP comet growth (before turning) from an imaginary line joining the comet's origin to the entrance of the axon (as indicated in (A)) within the soma of control neurons. A smaller angle represents growth towards the axon. (**E**) Graph shows the % of comets that enter the axon (green) or the dendrites (magenta) (including only those comets that grew towards the axon and dendritic entry sites) in either control (left) or Kinesin-2 RNAi (right) class I da neuron soma. (**F**) Graph shows the % of comets that are either anterograde (plus-end-out; blue) or retrograde (minus-end-out; red) in the proximal primary dendrite (before any branches) in either control (left) or Kinesin-2 RNAi (right) class I da neurons. (**G**) A model depicting microtubule nucleation and growth within soma of control (upper section) and Kinesin-2 depleted (lower section) da neurons. γ-TuRCs localise to the somatic Golgi and nucleate microtubules preferentially towards the axon (i). In control neurons, Kinesin-2 at the plus ends of growing microtubules can guide growing microtubules towards the axon along a polarised microtubule network (ii). Growing

microtubules readily enter axons (iii) but are excluded from entering dendrites (iv). This is because plus-end-associated Kinesin-2 engages with microtubules of opposite polarity and exerts a backward force that leads to stalling and depolymerisation of the growing microtubule. In Kinesin-2 depleted neurons, microtubules are still nucleated from the somatic Golgi but they grow in straight lines, because their plus ends are no longer guided (v), until contact with the nuclear envelope (vi) or the cell cortex (not depicted). Microtubules that approach dendrites can now readily enter (vii) due to the lack of engagement with dendritic microtubules.

STAR methods

Contact for Reagent and Resource Sharing

Further information and requests for resources and reagents should be directed to and will be fulfilled by the Lead Contact, Paul Conduit (ptc29@cam.ac.uk).

Experimental Model and Subject Details

All fly strains were maintained at 18 or 25°C on Iberian fly food made from dry active yeast, agar, and organic pasta flour, supplemented with nipagin, propionic acid, pen/strep and food colouring.

Drosophila melanogaster stocks

The following fluorescent alleles were used in this study: γ-tubulin23c-sfGFP (Tovey et al., 2018), γ-tubulin23c-eGFP (this study), sfGFP-Cnn-P1 (this study), sfGFP-Cnn-P2 (this study), UAS-mCD8-mRFP (BL 27392), UAS-EB1-GFP (BL 35512), UAS-ManII-mCherry (Susan Younger), and UAS-ManII-GFP (BL 65248). The following fluorescent gal4 lines were used in this study: ppk-Gal4 Chr II (B32078) and Chr III (BL 32079) and 221-Gal4 (BL 26259). The following mutant alleles were used in this study: plp^{5} (BL 9567), plp^{s2172} (BL 12089), cnn^{f04547} (Exelixis at HMS), ppkCD4 td GFP (BL 35842), KAP RNAi (VDRC 45400 GD).

For examining the endogenous localisation of γ-tubulin23C we used flies expressing γ-tubulin23C-sfGFP and γ-tubulin23C-eGFP i.e. 2 copies of γ-tubulin23C-GFP, either alone or in combination with one copy of UAS-mCD8-RFP expressed under the control of one copy of either 221-Gal4 or the ppk-Gal4. For examining the localisation of Cnn, we used flies expressing two copies of either sfGFP-Cnn-P1 or sfGFP-Cnn-P2 either alone or in combination with one copy of UAS-mCD8-RFP expressed under the control of one copy of either 221-Gal4 or the ppk-Gal4. For examining the localisation of Plp in relation to medial Golgi, we used flies with one copy of UAS-ManII-GFP expressed under the control of one copy of either 221-Gal4 or the ppk-Gal4. For examining the localisation of γ-tubulin23C in the absence of Cnn or Plp, we used flies expressing two copies of γ-tubulin23C-(sf/e)GFP (as above) in a $cnn^{f04547}/cnn^{f04547}$ or plp^{5}/plp^{s2172} mutant background. For examining microtubule dynamics we used flies with one copy of UAS-EB1-GFP expressed under the control of one copy of either 221-Gal4 or the ppk-Gal4. For examining microtubule dynamics in relation to the Golgi we used flies with one copy of UAS-EB1-GFP and one copy of UAS-ManII-mCherry, both expressed under the control of one copy of either 221-Gal4 or the ppk-Gal4.

Method Details

DNA cloning

5-alpha Competent *E. coli* (High Efficiency) (NEB) cells were used for bacterial transformations, DNA fragments were purified using QIAquick Gel Extraction Kits (Qiagen), plasmid purification was performed using QIAprep Spin Miniprep Kits (Quiagen). Phusion High-Fidelity PCR Master Mix with HF Buffer (ThermoFisher Scientific) was used for PCRs.

Generating endogenously-tagged fly lines

All endogenously-tagged lines were made using CRISPR combined with homologues recombination, by combining the presence of a homology-repair vector containing the desired insert with the appropriate guide RNAs and Cas9. The *γ-tubulin23C-eGFP* allele was generated by inDroso by initially inserting an SSSS-eGFP-3'UTR-LoxP-3xP3-dsRED-Lox P cassette before the selection markers were excised. The multi-serine insert acts as a flexible linker between γ-tubulin23C and eGFP. The following guide RNA sequences were used to cut either side of the 3'UTR: AGTCGATClTGTGACCAGCGC and TTATGGTTlAATGTCGACTTG. The sfGFP-Cnn-P1 (insertion of sfGFP at the start of exon 1a) and sfGFP-Cnn-P2 (insertion of sfGFP at the start of exon 1b) alleles were generated within the lab following the approach used previously[58]. Briefly, flies expressing a single guide RNA (either GTCGTGTTTAGACTGGTCCATGGG for Cnn-P1 or GTCGTTAAATGAAACATAGAATA for Cnn-P2) were crossed to nos-Cas9 expressing females and the resulting embryos were injected with a pBluescript plasmid containing sfGFP and linker sequence (4X GlyGlySer) flanked on either side by 1.5kb of DNA homologous to the *cnn* genomic locus surrounding the 5' end of the appropriate coding region. The homology vectors were made by HiFi assembly (NEB) of PCR fragments generated from genomic DNA prepared from nos-Cas-9 flies (using MicroLYSIS, Microzone) and a vector containing the sfGFP tag (DGRC, 1314). Homology vectors were injected into embryos by the Department of Genetics Fly Facility, Cambridge, UK. F1 and F2 males were screened by PCR using the following primers: for sfGFP-Cnn-P1: forward primer: AAAGTTAACTATTTGAGGACCTCCCATGGTGTCCAAGGGCGAGGAG; reverse primer: CCCGCAAAACCTGTTTAGACTGGTCGGATCCGCCGCTACCTCCGCTTCCACCGGAACC TCCCTTGTACAGCTCATCCATGCC; for sfGFP-Cnn-P2: forward primer: GCAAATGTTAAATGAAAGATACAATATGGTGTCCAAGGGCGAGGAG; reverse primer: GTGAGGTAGATCGAAAGATACCCGCGGATCCGCCGCTACCTCCGCTTCCACCGGAAC CTCCCTTGTACAGCTCATCCATGCC.

Antibodies

The following primary antibodies were used: anti-GFP mouse monoclonal at 1:250 (Roche, 11814460001), anti-Cnn Rabbit polyclonal raised against first 660aa of Cnn-P1 (which includes amino acids 35-632 of Cnn-P2) at 1:1000[64], anti-Plp rabbit polyclonal at 1:500[92], Alexa647 conjugated HRP polyclonal at 1:500 (Jackson), and anti-GM130 rabbit polyclonal at 1:300 (Abcam). The following secondary antibodies were used: ATTO-488 GFP-booster at 1:200 (Chromotek), Alexa-488 anti Mouse at 1:500 (ThermoFisher), Alexa-547 anti Rabbit at 1:500 (ThermoFisher).

Immunostaining

Larvae were dissected as described previously[93]. The fillet preps were fixed in freshly prepared 4% formaldehyde for 20 minutes at room temperature and were then washed four times for 10 minutes in PBST (PBS + 0.1% TritonX-100). The preps were then blocked in PBST + 5% BSA for 1h at room temperature and incubated with the appropriate primary antibodies diluted in PBST overnight at 4°C. After washing in PBST for the whole day, changing washes every 30-45 minutes, samples were incubated in secondary antibodies diluted in PBST overnight at 4°C. The fillet preps were then washed for the whole day, changing washes every 30-45 minutes in PBST before mounting in Moviol. They were stored at -20°C and imaged within a week.

Fixed and live cell imaging

Imaging of all samples except for those expressing EB1-GFP or GFP-Cnn-P1 was carried out on an Olympus FV3000 scanning inverted confocal system run by FV-OSR software using a 60X 1.4NA silicon immersion lens (UPLSAPO60xSiicon). For live samples, wandering L3 larvae were placed in a drop of glycerol and flattened between a slide and a 22X22mm coverslip, held in place by double-sided sticky tape, and imaged immediately. Imaging of EB1-GFP within da neurons and GFP-Cnn-P1 within embryos was performed on a Leica DM IL LED inverted microscope controlled by μManager software and coupled to a RetigaR1 monochrome camera (QImaging) and a CoolLED pE-300 Ultra light source using a 63X 1.3NA oil objective (Leica 11506384). For EB1-GFP imaging, larvae were dissected in live imaging solution (ThermoFisher) to remove the majority of their insides and mounted in Schneider's media supplemented with FBS and Pen/strep between a slide and 22X22mm coverslip held in place with tape and imaged immediately. When using the CherryTemp, the larvae were held between the CherryTemp chip and a 22X22mm coverslip. The CherryTemp software was used to rapidly change the temperature of the liquid within the flow chamber from 20°C to 5°C

after an initial 45s of imaging. The temperature was then rapidly changed back to 20°C after a further 180s and the neurons were imaged for a further 135s. For all EB1-GFP imaging, single Z-plane Images were acquired every 3 seconds. All images were processed using Fiji (ImageJ). EB1 comets were tracked using the Manual tracking plugin in Fiji.

Quantification and Statistical Analysis

Statistical analysis and graph production were performed using GraphPad Prism. For EB1-comet analysis, we excluded comets that were present within the first timepoint (and thus may not represent newly growing microtubules). The angle of initial comet growth was measured using the angle tool within imageJ, by drawing lines from the axon entry site to the comet origin and then along the intial linear path of the comet. To assess whether comets approached axons or dendrites, we defined a region of the soma adjacent to the axon or dendrites and counted comets that entered this region as comets that had approached with the axon or dendrites. We scored comets as entering the axon or dendrites if they passed this region and grew even a short distance into the axon or dendrite. N numbers were as follows: 9 larvae, imaged for an average of 267s. An average of 44.4 comets per neuron were observed with an average of 28 per neuron originating within the soma. An average of 21 comets per neuron stopped before reaching the axon or soma, with an average of 5 comets per neuron reaching the axon and 2 comets per neuron reaching the dendrites.

Supplementary Figure legends

Figure S1 – related to Figure 1

Ectopically expressed γ-tubulin-GFP is strongly enriched in branchpoints and dendritic bubbles and ectopically expressed ManII is not a reliable marker of Golgi outposts in class I da neurons. (**A**) Fluorescent confocal images of the proximal region of a class I da neuron expressing 221-gal4>UAS-γ-tubulin-GFP (green) and 221-gal4>UAS-ManII-mCherry (magenta) within a living 3rd instar larvae. Left panel shows an overlay of the GFP and mCherry channels, middle and right panels show the GFP and mCherry channels, respectively. Blue and orange arrowheads indicate enrichments of ectopically expressed γ-tubulin-GFP within branchpoints and dendritic bubbles, respectively. (**B**) Fluorescent confocal images of distal dendrites from different class I da neurons expressing 221-gal4>UAS-ManII-GFP fixed and immunostained with antibodies against HRP (greyscale). Arrowheads indicate HRP puncta that represent internal membrane, at least some of which could be Golgi outposts. Note how UAS-ManII-GFP spreads into regions of the class I dendrites, including dendritic bubbles, that do not contain HRP puncta, suggesting that over-expressing ManII in class I neurons leads to 'leaking' of the protein outside of Golgi outposts.

Figure S2 – related to Figure 3

Endogenously-tagged γ-tubulin-GFP localises to the somatic Golgi of sensory neurons. (**A,B**) Confocal images show the soma of an external sensory neuron (A) or another sensory neuron within the dorsal cluster (B) from 3rd instar larvae expressing two copies of endogenous γ-tubulin-GFP fixed and immunostained with antibodies against GFP (green), GM130 (magenta) and HRP (greyscale). γ-tubulin-GFP and GM130 signals associate at presumptive side-on stacks (extended GM130 signal) and end-on stacks (round GM130 signal) in a way that suggests γ-TuRCs are recruited to the outer face of the cis-Golgi.

Figure S3 – related to Figure 4

Cnn-P1 is not strongly associated with the somatic Golgi or Golgi outposts of sensory neurons, while Cnn-P2 is expressed in ensheathing Glia . (**A**) A gene diagram of *cnn* to indicate the different Cnn isoforms. Boxed regions are exons, lines are introns. CRISPR combined with homologous recombination was used to insert GFP just after the start codon of either the promoter 1 (P1) or promoter 2 (P2) isoform. Promotor three isoforms are expressed only in testis and so were not analysed in this study. (**B**) Confocal images show the somas and some proximal dendrites of sensory neurons within the dorsal cluster from a 3rd instar larva expressing endogenously-tagged GFP-Cnn-P1 and immunostained with nanobodies against GFP covalently coupled to atto-488 (green) and antibodies against HRP (greyscale) and GM130 (magenta). Left panel (B) shows an overlay of the GFP and anti-HRP signals, while the right panel (B') shows the GFP signal with coloured outlines of the different neurons drawn for convenience, with insets showing all channels, including an overlay, for the class I neuron soma, regions of the class IV neuron soma and a class IV proximal branchpoint that contains Golgi outposts. The GFP-Cnn-P1 signal appears very weakly, if at all, at the somatic Golgi and Golgi outposts marked by HRP and GM130 staining. (**C**) Confocal images show class I da neurons from a 3rd instar larva expressing 221-Gal4>UAS-mCD8-RFP (magenta) and two copies of endogenously tagged GFP-Cnn-P2. Left panel (C) shows an overlay of the GFP and RFP channels, while the right panel (C') shows just the GFP channel. Note how the GFP-Cnn-P2 surrounds the axons and somas of the neurons, suggestive of localisation within ensheathing glia. The * star indicates a region of very bright RFP signal that has bled through into the GFP channel.

Figure S4 – related to Figure 5

Plp localises to the somatic Golgi, Golgi outposts, basal bodies and class I -specific dendritic bubbles.

(**A**) Confocal images show the somas and some proximal dendrites of sensory neurons within the dorsal cluster from a 3rd instar larva expressing ppk-mCD4-tdGFP and immunostained with antibodies against GFP (green), HRP (greyscale) and Plp (magenta). Left panel (A) shows the GFP and anti-HRP channels, while the right panel (A') shows the anti-Plp channel; insets show an overlay of the anti-Plp and anti-HRP

channels. Plp signal colocalises with the HRP staining that marks the multiple well-distributed Golgi stacks within the neuronal soma of each neuron. Plp also localises to some HRP puncta (presumably Golgi outposts) within the proximal branchpoints of class IV neurons. Note that Plp antibodies also strongly stain other nearby epidermal and muscle cells. (**B**) Confocal images show parts of the external sensory neurons containing the basal bodies from a 3rd instar larva expressing two copies of endogenously tagged γ-tubulin-GFP and immunostained with antibodies against GFP (green), HRP (greyscale) and Plp (magenta). (**C**) Confocal images show dendritic bubbles of a class I da neuron from a 3rd instar larva expressing immunostained with antibodies against HRP (greyscale) and Plp (magenta).

Supplementary Movie Legends

Movie S1 – related to Figure 4.

Endogenously-tagged GFP-Cnn-P1 localises as expected to centrosomes within *Drosophila* syncytial embryos. The Movie was taken using multi-Z-stack time-lapse epifluorescence microscopy and shows Z-projected images through time of a syncytial embryo expressing endogenously-tagged GFP-Cnn-P1. The cycle starts in M-phase and the centrosomes separate when the cycle transitions to the following S-phase. GFP-Cnn-P1 localises to centrosomes during both M-phase, where the signal is rounded, and S-phase, where the signal displays the typical Cnn flares previously observed with both immunostaining and ectopic GFP-Cnn-P1 expression. Images were collected every 20s and the Movie plays at 20 frames/second.

Movie S2 – related to Figure 6.

EB1-comets emerge from somatic Golgi stacks. The Movie was taken using single-Z time-lapse epifluorescence microscopy and shows a class I da neuron expressing 221-Gal4>UAS-EB1-GFP and 221-Gal4>UAS-ManII-mCherry. The left panel shows an overlay of the GFP and mCherry channels, while the right panel shows the same overlay with the imageJ-generated EB1-GFP comet tracks drawn onto the images. The tracks are multi-coloured, as is default for imageJ, and the colours have no reference to comet type. Comets can be seen emerging from Golgi stacks and and this can occur repeatedly from the same stack (see bottom right stack). Images were collected every 3s and the Movie plays at 10 frames/second.

Movie S3 – related to Figure 6.

The somatic Golgi stacks nucleate microtubules. The Movie was taken using single-Z time-lapse epifluorescence microscopy and shows a class I da neuron expressing 221-Gal4>UAS-EB1-GFP and 221-Gal4>UAS-ManII-mCherry. The sample was subjected to a warming-cooling-warming (20˚C-5˚C-20˚C) cycle, as indicated by the red (20˚C) and blue (5˚C) borders. The left panel shows an overlay of the GFP and mCherry channels, while the right panel shows the same overlay with the imageJ-generated EB1-GFP comet tracks drawn onto the images. The tracks have been manually post-coloured such that green comets represent comets emerging from

Golgi stacks and purple comets represent comets emerging from elsewhere within the soma. Comets can be seen emerging from Golgi stacks before cooling, and then all comets stop during the 3 minute cooling period. After warming, comets can be seen emerging from the Golgi stacks, including comets that emerge >1min after warming. Images were collected every 3s and the Movie plays at 10 frames/second.

Movie S4 – related to Figure 7.

Microtubules grow preferentially towards the axon and are excluded from entering dendrites. The Movie was taken using single-Z time-lapse epifluorescence microscopy and shows a control class I da neuron expressing 221-Gal4>UAS-EB1-GFP. The left panel shows the GFP channel, while the right panel shows the GFP channel with the imageJ-generated EB1-GFP comet tracks drawn onto the images. The tracks are multi-coloured, as is default for imageJ, and the colours have no reference to comet type. Comets can be seen emerging from multiple locations within the soma but have a preference to initially grow towards the axon (quantified in Figure 7). Comets also display turning events, indicating that the growing plus ends of microtubules can be guided along pre-existing microtubules. Comets that approach the axon frequently enter and grow down the axon; In contrast, comets that approach a dendrite entry site do not enter (quantified in Figure 7). Images were collected every 5s and the Movie plays at 10 frames/second.

Movie S5 – related to Figure 7.

Kinesin-2 is required for growing microtubules to turn within the soma and to be excluded from entering dendrites. The Movie was taken using single-Z time-lapse epifluorescence microscopy and shows a Kinesin-2 RNAi class I da neuron expressing 221-Gal4>UAS-EB1-GFP and 221-Gal4>UAS-Kap3-RNAi. The left panel shows the GFP channel, while the right panel shows the GFP channel with the imageJ-generated EB1-GFP comet tracks drawn onto the images. The tracks are multi-coloured, as is default for imageJ, and the colours have no reference to comet type. Comets can be seen emerging from multiple locations within the soma but unlike in control neurons they do not turn unless they encounter the nuclear envelope or cell cortex, suggesting that Kinesin-2 is required to guide growing microtubules towards

the axon. Comets that approach the axon still frequently enter and grow down the axon, and, in contrast to control neurons, comets that approach dendrites also readily enter (quantified in Figure 7). This shows that Kinesin-2 is also required for excluding growing microtubules from entering dendrites. Images were collected every 5s and the Movie plays at 10 frames/second.

Movie S6 – related to Figure 7.

Growing microtubule minus ends appear to enter dendrites. The Movie was taken using single-Z time-lapse epifluorescence microscopy and shows a class I da neuron expressing 221-Gal4>UAS-EB1-GFP. The left panel shows the GFP channel, while the right panel shows the GFP channel with the imageJ-generated EB1-GFP comet tracks drawn onto the images. The tracks are multi-coloured, as is default for imageJ, and the colours have no reference to comet type. Arrowheads in the left panel indicate what appears to be a comet splitting event, suggestive of a microtubule simultaneously growing at both its plus and minus end. The green arrowhead marks the comet that grows into a dendrite. This comet moves slightly slower than the comet marked by the blue arrowhead, indicating that it is the minus end. Another comet, which does not appear from a splitting event, also grows into a dendrite (pink comet – from 01:18 to 02:30); this may therefore be one of the rare plus ends that enters a dendrite. Images were collected every 5s and the Movie plays at 10 frames/second.

Figure 1

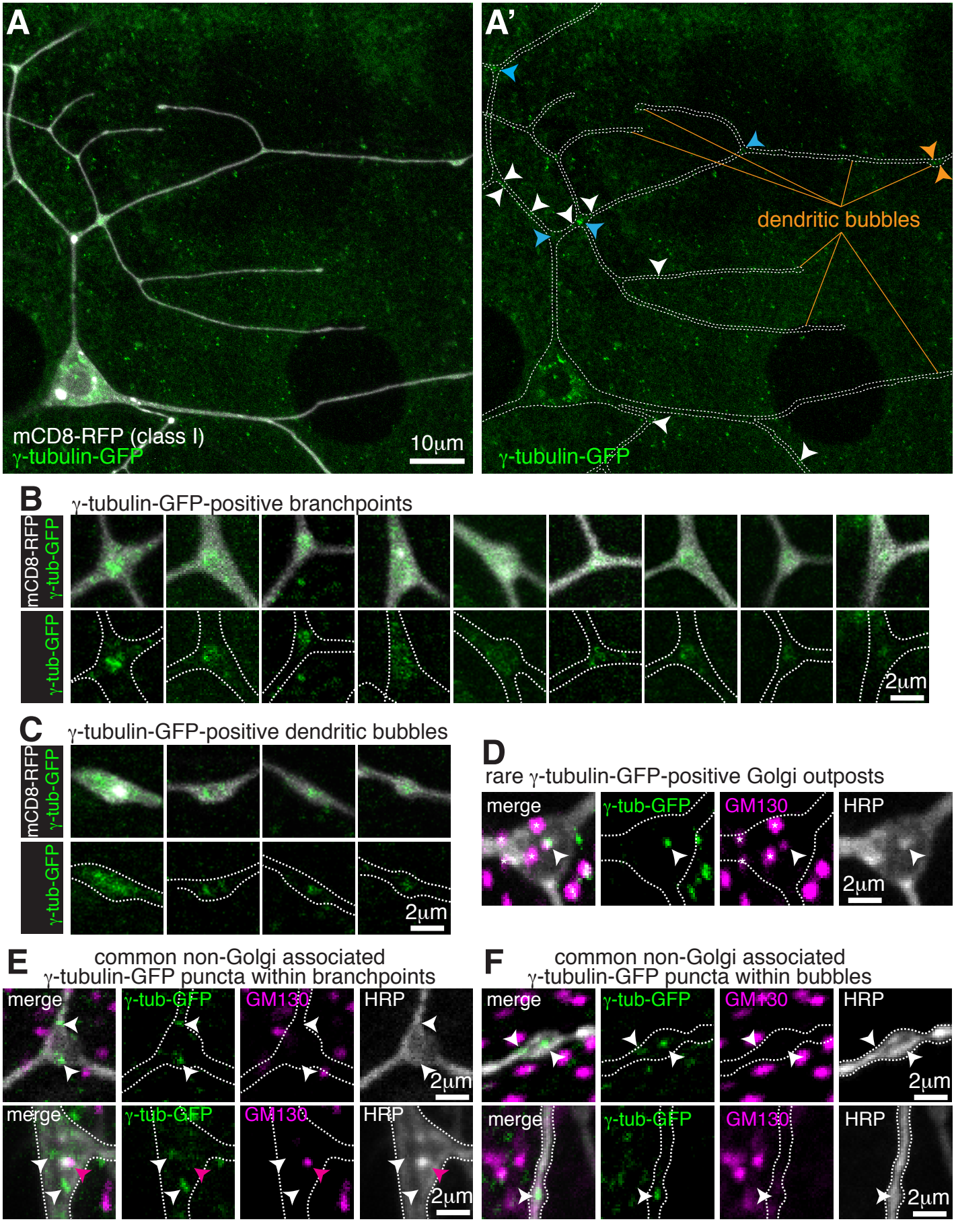

Figure 2

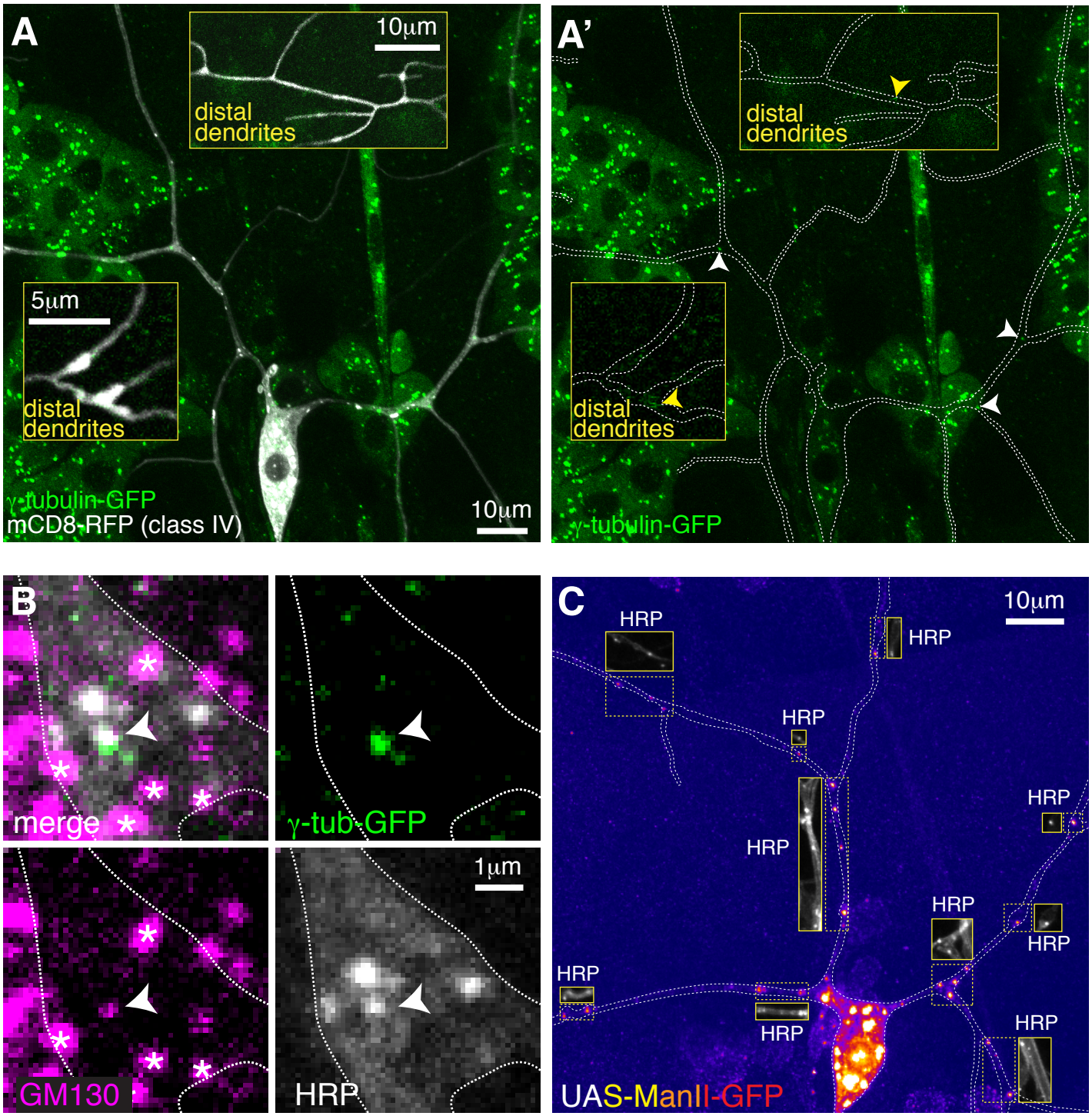

Figure 3

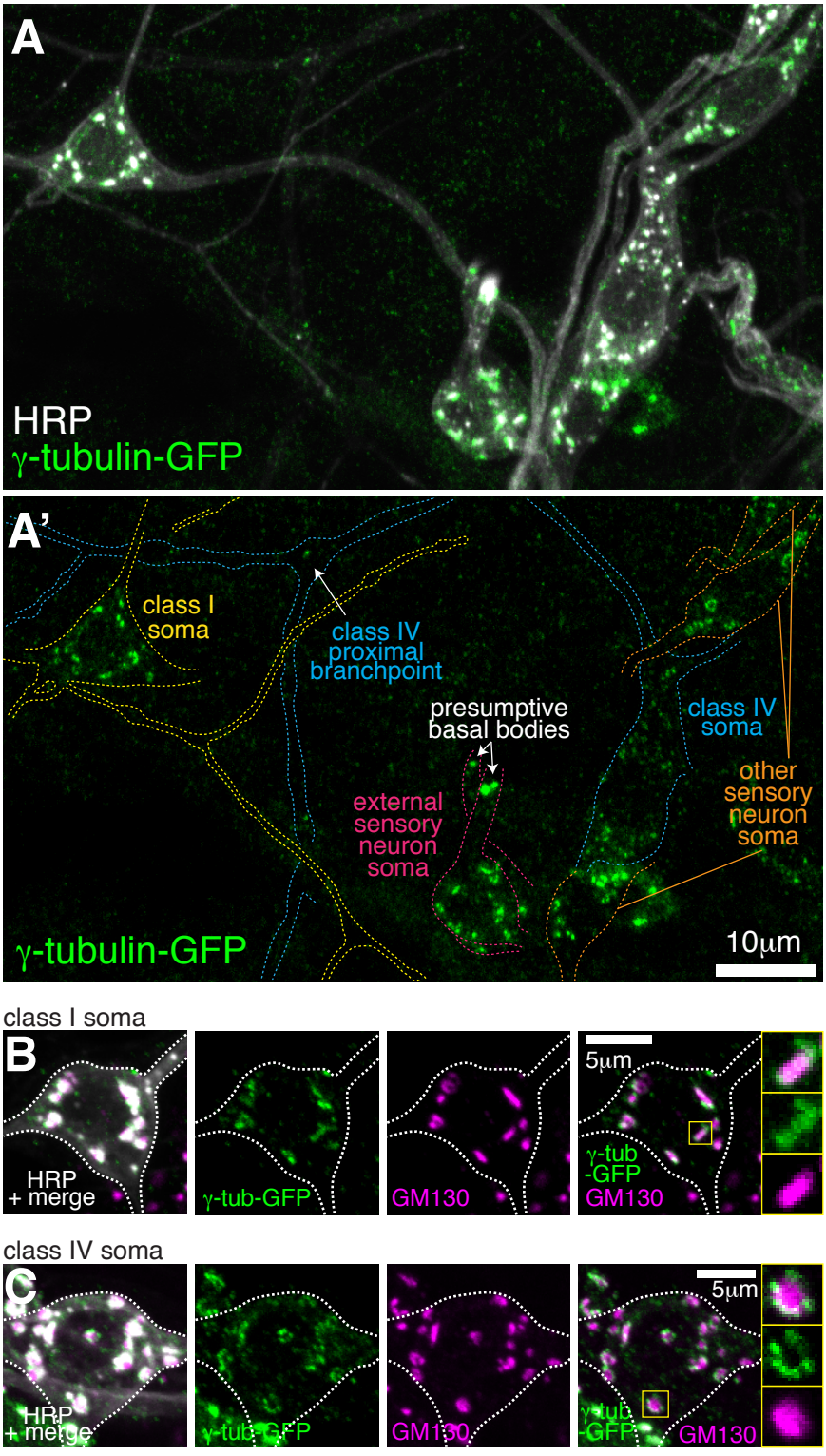

Figure 4

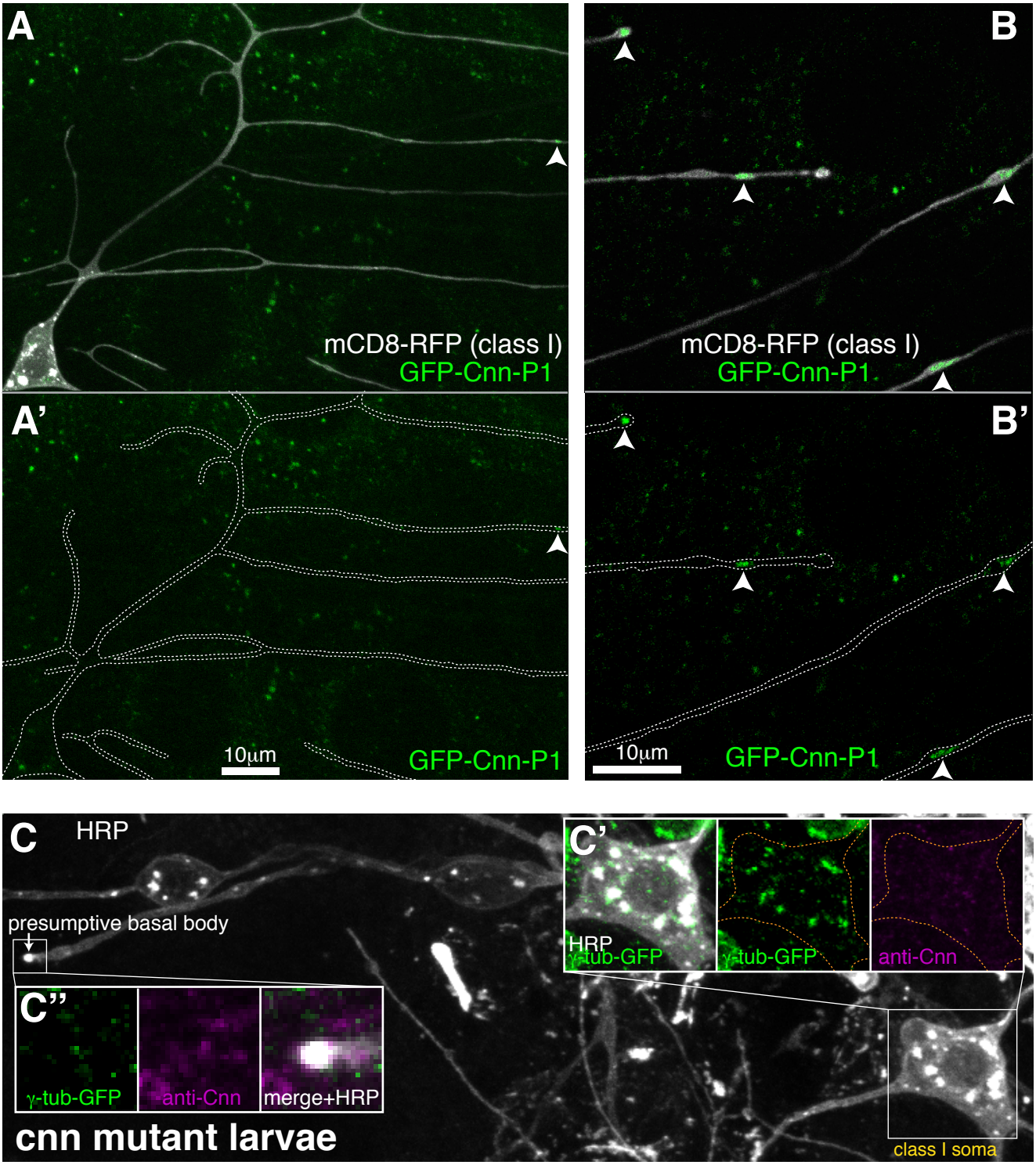

Figure 5

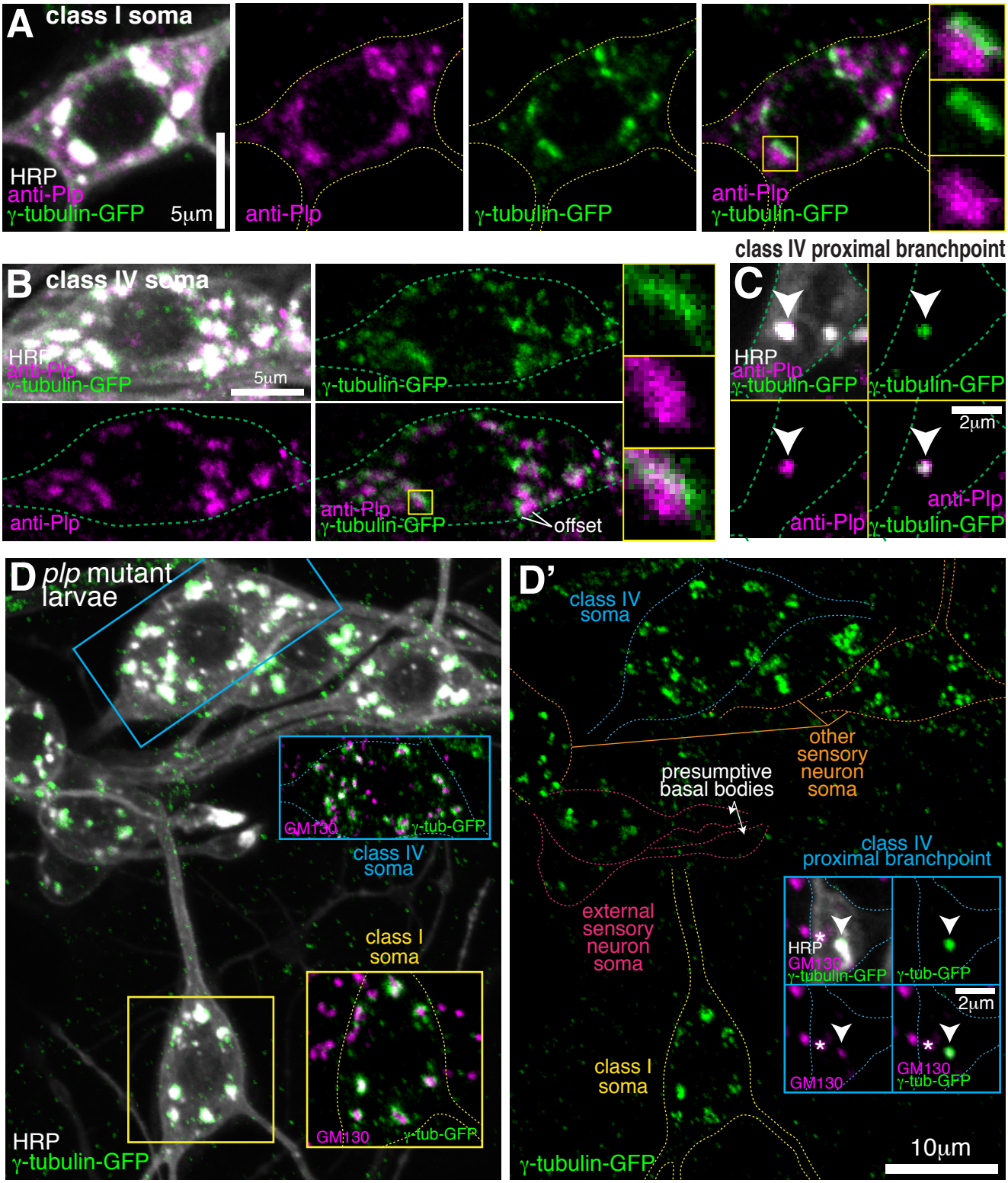

Figure 6

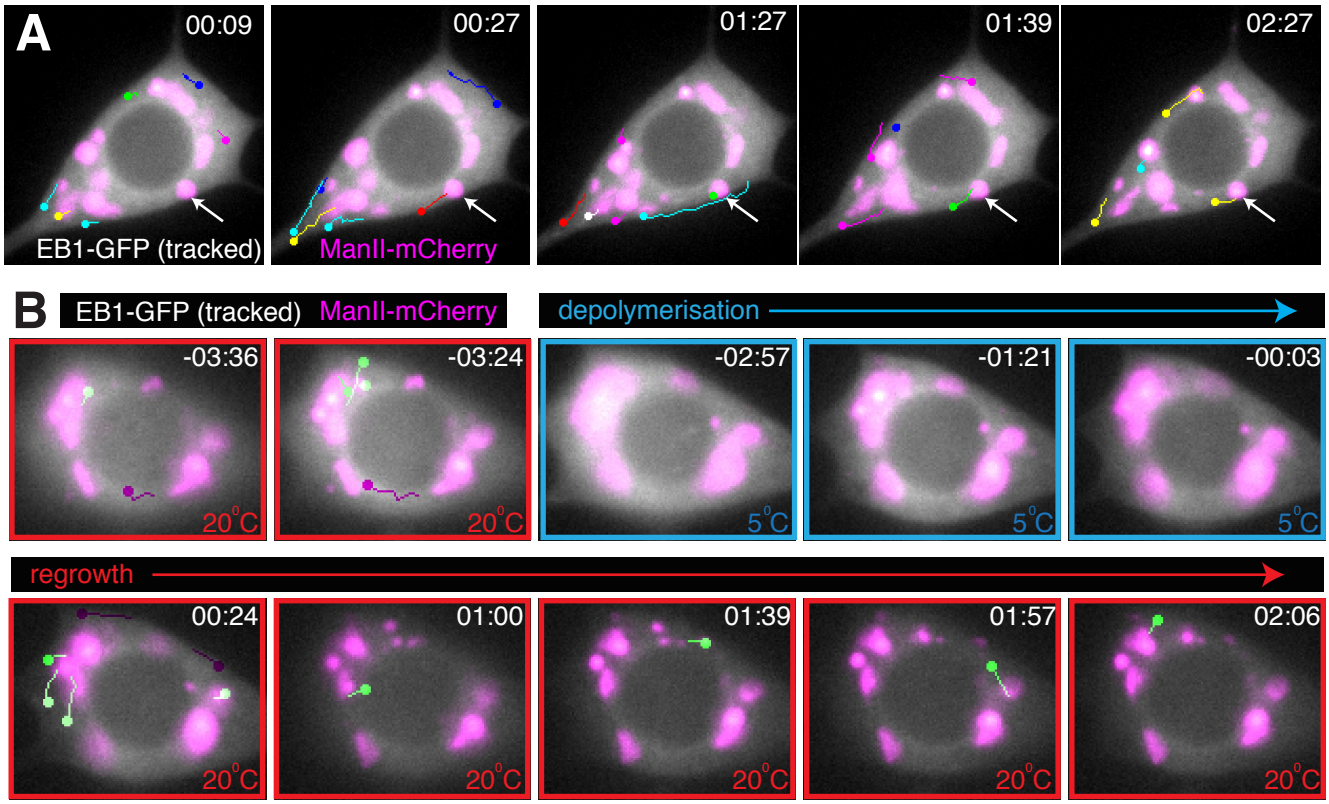

Figure 7

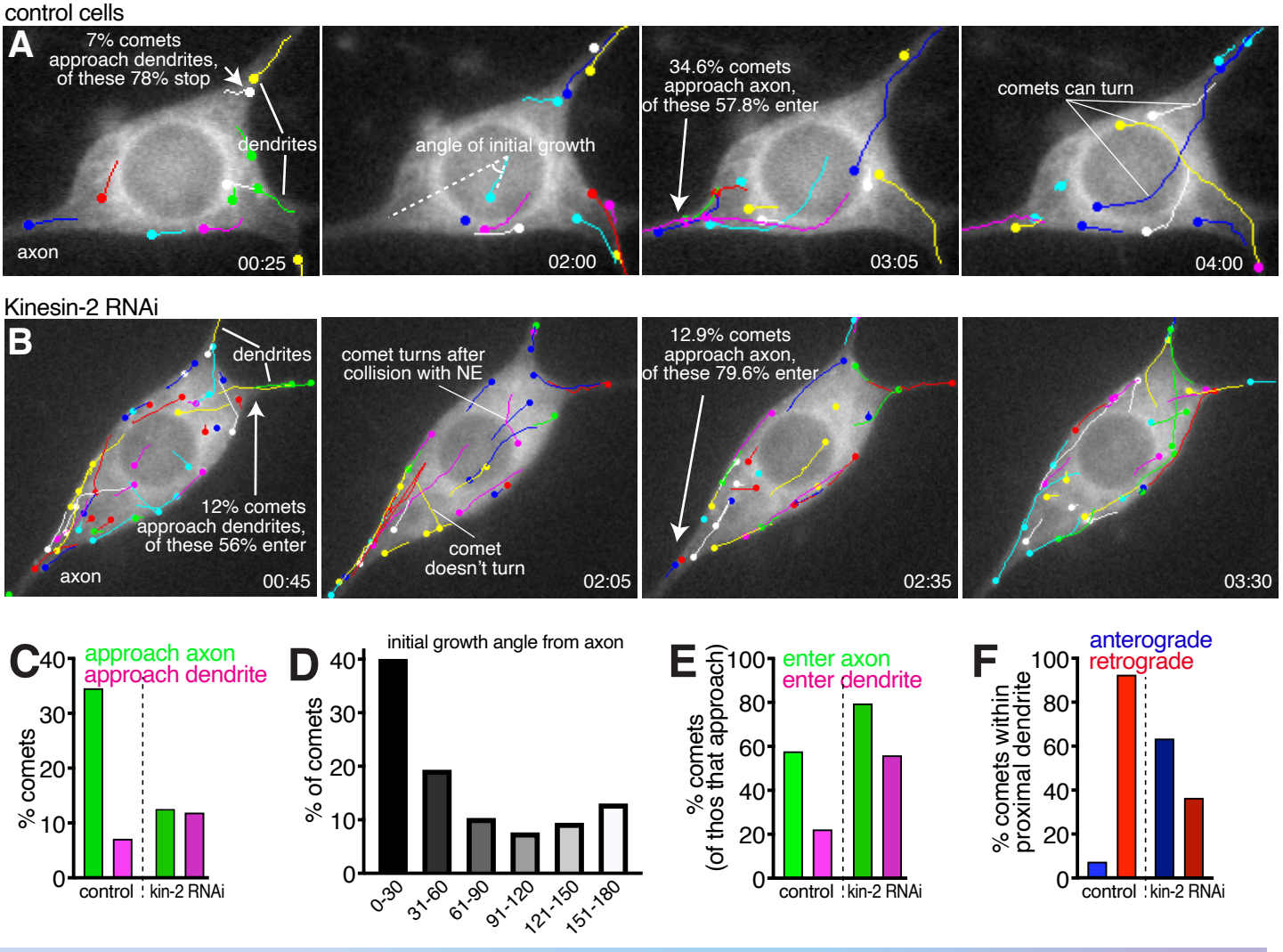

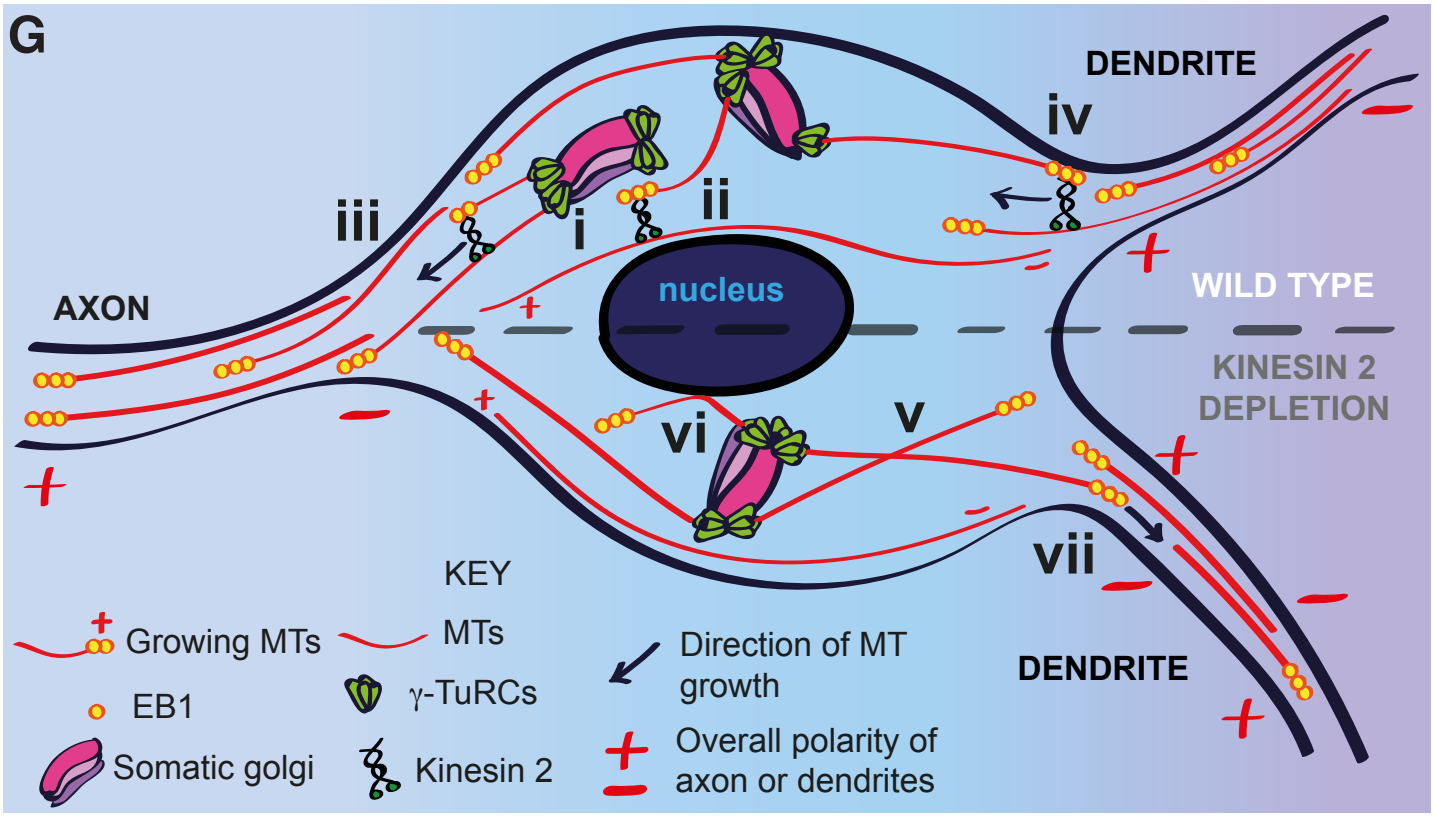

Figure S1

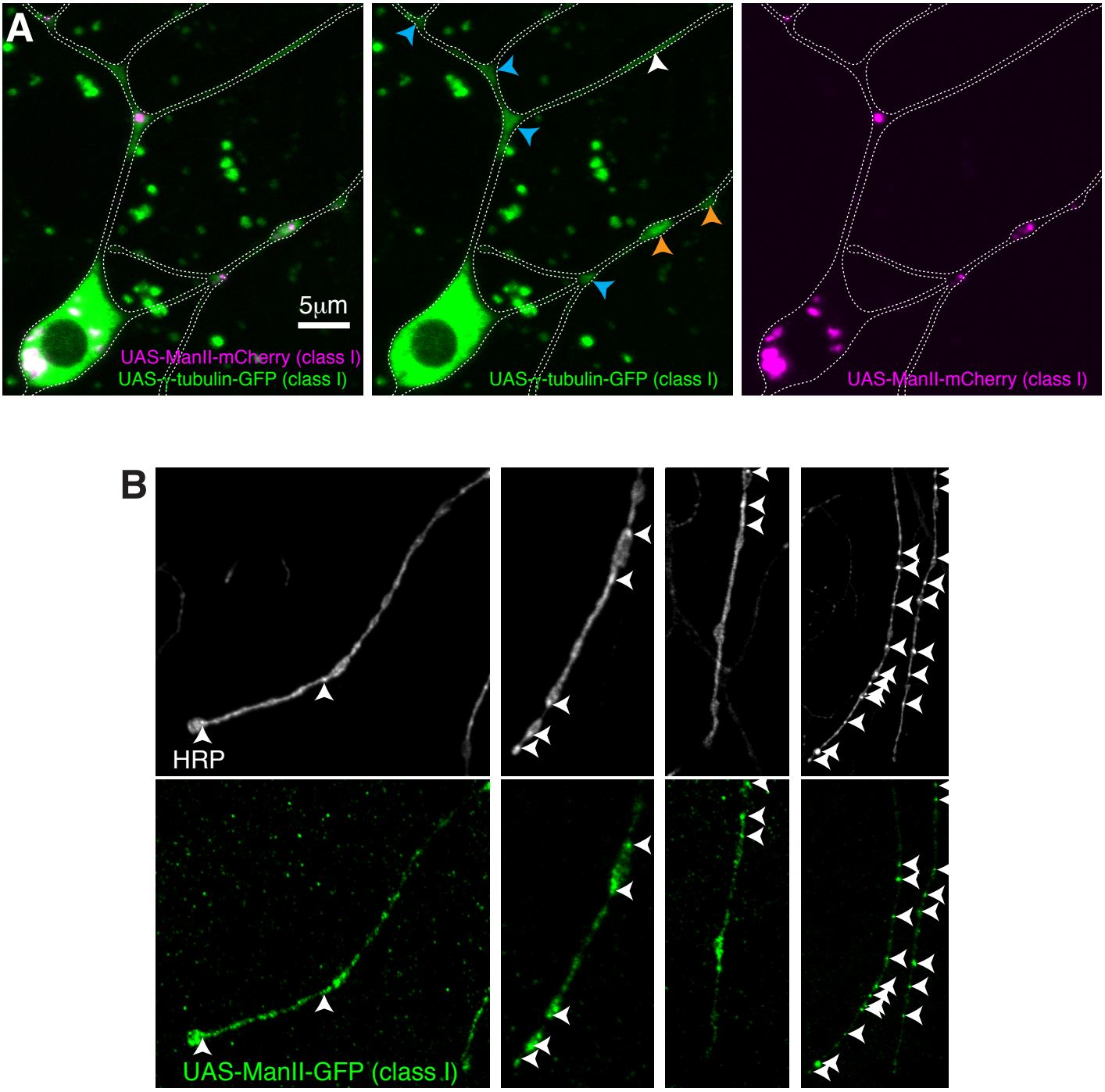

Figure S2

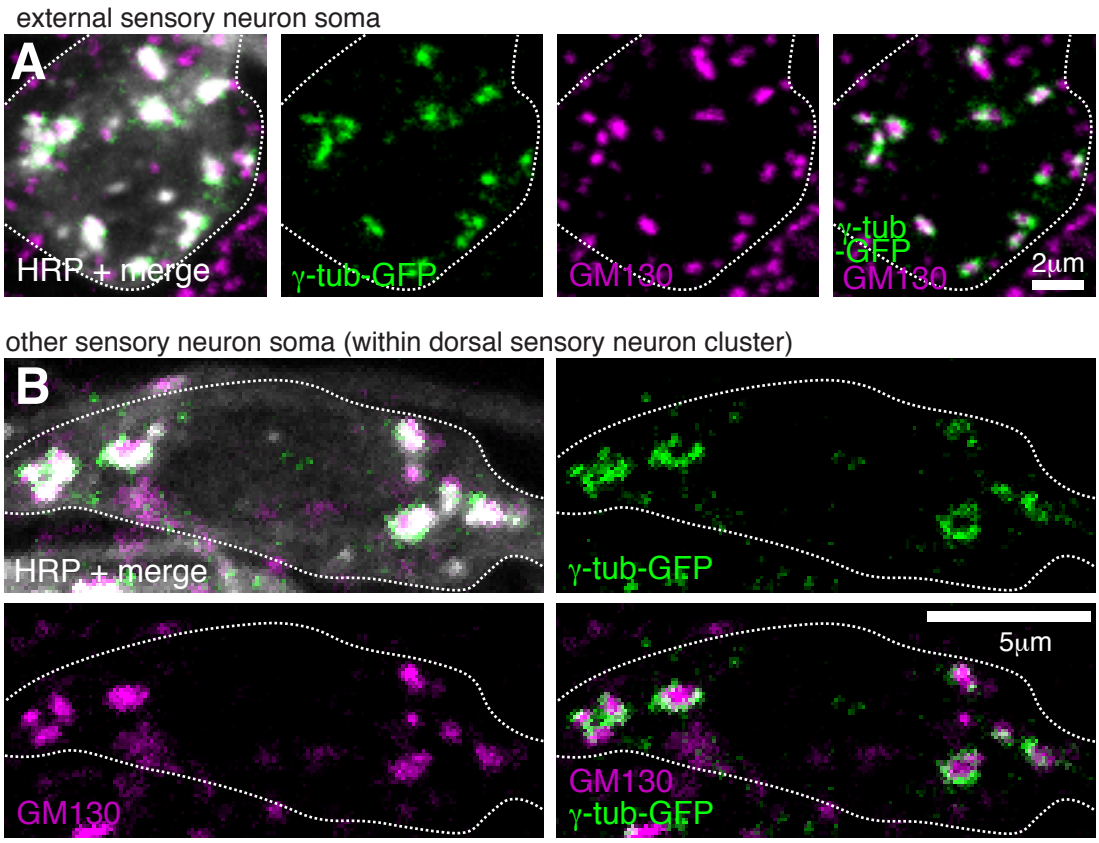

Figure S3

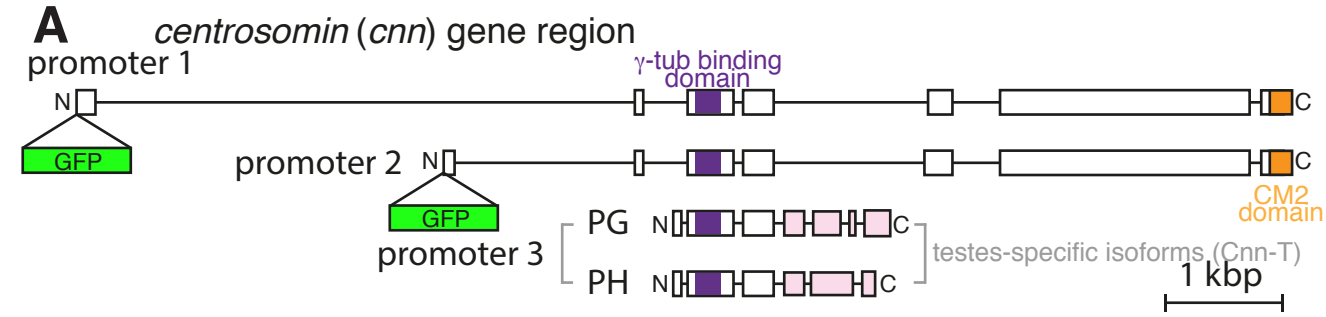

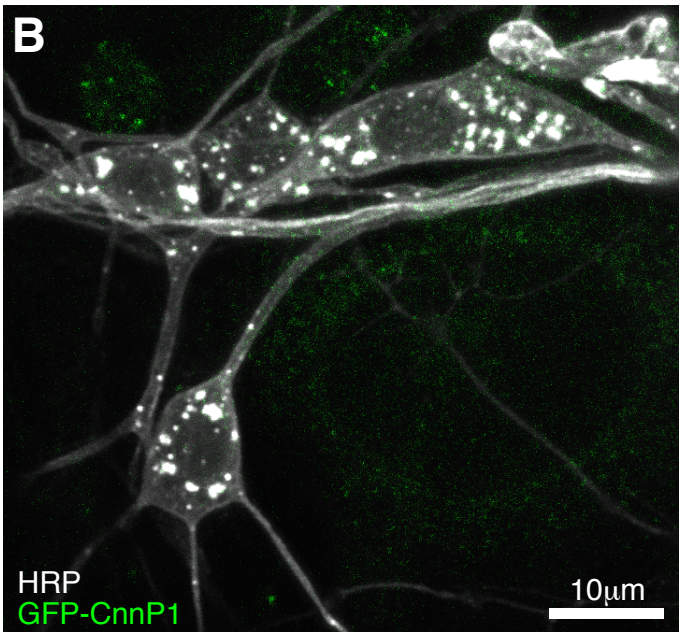

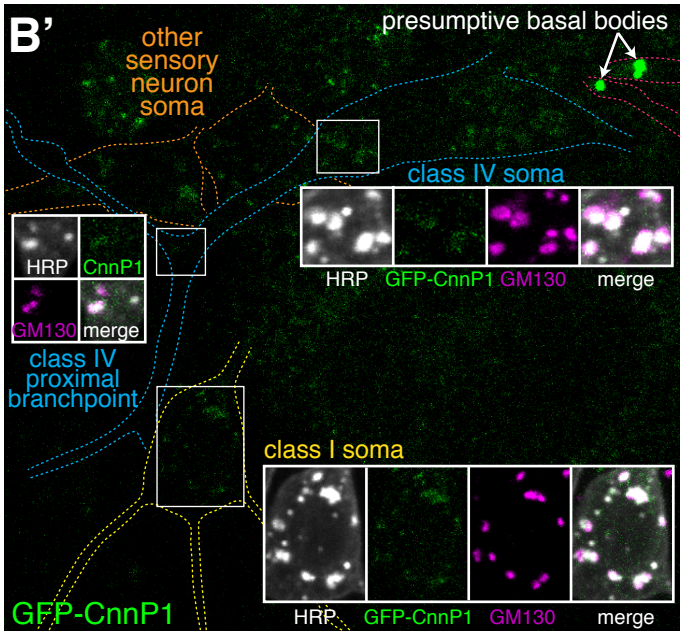

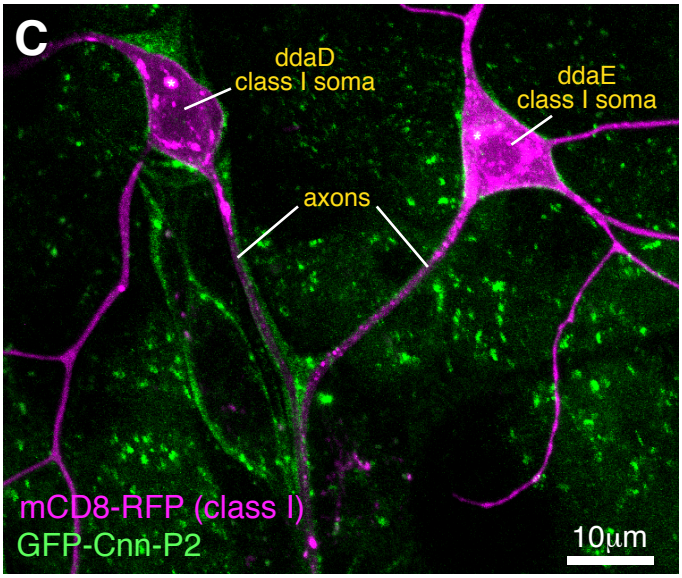

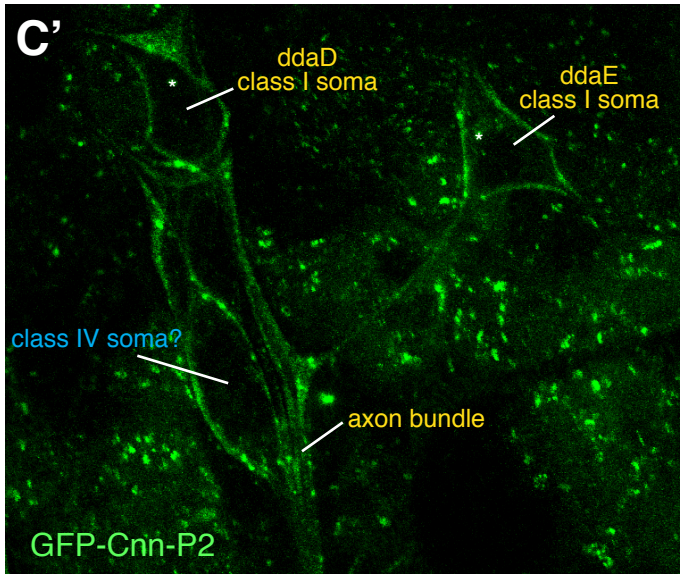

Figure S4